MICROSCOPIC ANALYSIS OF WOBBLING EXCITATIONS IN ^{156}Dy AND ^{162}Yb

R. G. Nazmitdinov[*]

Departament de Física, Universitat de les Illes Balears
E-07122, Palma de Mallorca, Spain

Bogoliubov Laboratory of Theoretical Physics, Joint Institute for Nuclear Research
141980, Dubna, Moscow Region, Russia

J. Kvasil

Institute of Particle and Nuclear Physics, Charles University
CZ-18000, Praha 8, Czech Republic

In the cranked Nilsson-plus-random-phase approximation, we study low-lying quadrupole excitations of positive parity and negative signature in ^{156}Dy and ^{162}Yb at high spins. Special attention is paid to a consistent description of wobbling excitations and their identification among excited states. A good agreement between the available experimental data and the results of calculations is obtained. We find that the lowest odd-spin γ-vibrational states in ^{156}Dy transform into the wobbling excitations after the backbending associated with the transition from axially symmetric shape to nonaxial shape. Similar results are predicted for ^{162}Yb. The analysis of electromagnetic transitions uniquely determines the sign of γ-deformation in both nuclei after the transition point.

PACS: 21.10.Re, 21.60.Jz, 27.70.+q

1. INTRODUCTION

Deformation is an important ingredient of nuclear dynamics at low energies [1, 2]. Regular rotational bands identified in spectroscopic data are most evident and prominent manifestations of an anisotropy of the spatial nuclear density distribution. While the axial deformation of the nuclear potential is well established, there is a long-lasting debate on the existence of a triaxial deformation. The full understanding of this degree of freedom in nuclei may have implications for other mesoscopic systems as well. In particular, the importance of nonaxiality is discussed recently for metallic clusters [3] and atomic condensates (see Ref. [4] and the references therein).

The analysis of specific low-lying excited states near the yrast line could shed light on the existence of nonaxiality. For nonaxial shapes, one expects the appearance of low-lying vibrational states associated with a classi-

cal wobbling motion. Such excitations (called wobbling excitations) were first suggested by Bohr and Mottelson in rotating even–even nuclei [1], and were then analyzed within simplified microscopic models [5, 6] (see also Ref. [7] and the references therein). According to the microscopic approach [8, 9], the wobbling excitations are vibrational states of negative signature built on the positive-signature yrast (vacuum) state. Their characteristic feature is the collective E2 transitions with $\Delta I = \pm 1\hbar$ between these and yrast states. First experimental evidence of such states in odd Lu nuclei was reported only recently [10].

The properties of the wobbling excitations at different angular momenta can be studied within the asymmetric rotor model (ARM) [1] (also see the Appendix). The extension of this model to odd nuclei was used recently for the analysis [11] of experimental properties of the second triaxial superdeformed band in ^{163}Lu, which carries several features associated with the wobbling excitations. The classical dispersion equation for

[*]E-mail: rashid@theor.jinr.ru, vdfsrna9@uib.es

the wobbling mode [1], with irrotational moments of inertia, was used to describe the spectrum. The moments of inertia were fitted in order to reproduce the experimental data. But the intepretation of the results with irrotational moments of inertia [11] faces the problem of a consistent description of data. It seems that the approach suggested in Ref. [11] may explain some tendencies, but these are only a crude approximation to the full physical picture of the observed phenomenon.

To explain the same data in ^{163}Lu, a non-self-consistent microscopic analysis based on the cranked Nilsson potential was performed in [12, 13]. As a basic tool, the dispersion equation for wobbling excitations, derived in the time-dependent Hartree–Bogoliubov approach in Ref. [9], has been used. Based on the solution of the microscopic equation, it was found in Ref. [13] that the wobbling excitations are very sensitive to a single-particle alignment. It was also concluded that the pairing correlations do not affect the wobbling excitations, and this should be considered a specific feature related to this mode. This seems to contradict the fact that alignment reduces the pairing correlations. Furthermore, the authors admitted that the kinematic moment of inertia $\mathcal{J}_x$ was not described properly (see Ref. [13]).

We recall that wobbling excitations depend on all three moments of inertia that characterize the nonaxial shape. Therefore, a self-consistent description for moments of inertia is a prerequisite for the microscopic analysis of the nuclear wobbling motion. The main aim of this paper is to analyze new data on high-spin states in ^{156}Dy and ^{162}Yb [14, 15] within a self-consistent microscopic approach [16]. Our calculations suggest that some excited states at high spins may represent wobbling excitations.

Our approach (CRPA) [16] amounts to a self-consistent solution of the cranked Nilsson potential for the yrast line and the analysis of the low-lying excitations near the yrast line in the random-phase approximation (RPA). The analysis of M1-excitations [17], shape–phase transitions, and the behavior of positive-signature excitations at backbending [16] confirmed the importance of self-consistency for the description of moments of inertia. We provide a refined microscopic description of the wobbling excitations in a time-independent uniformly rotating (UR) frame. In numerical analysis, we pay attention to the self-consistency between the mean field, vibrational excitations, and their electromagnetic properties. We recall that all negative-signature excitations, including the wobbling ones, are considered in the UR frame. To identify the wobbling excitations in experimental data, a few criteria are proposed in the literature, such as a large collectivity and zig-zag behavior of the $B(E2)$ transition probability from a given band into the yrast one with $\Delta I = \pm 1$, when one of the transitions is almost dominant [18]. We present a microscopic procedure that gives a definite answer as to how to identify the wobbling excitations. This procedure includes the analysis of inertial properties and $B(E2)$- and $B(M1)$-transitions probabilities.

The paper is organized as follows. In Sec. 2, we briefly review the main details of our approach (which is thoroughly discussed in Ref. [16]). In Sec. 3, we study the lowest negative-signature RPA excitations. The main focus in this section is on the definition of the specific characteristics associated with the wobbling mode. The conclusions are finally drawn in Sec. 4. To complete the analysis, we review properties of the wobbling mode in the ARM in the Appendix.

2. THE MODEL

2.1. Basic properties of the mean-field approximation

Our description is based on the Hamiltonian defined in the UR frame as

$$\hat{H}_\Omega = \hat{H} - \hbar\Omega\hat{J}_x = \hat{H}_0 - \sum_{\tau=n,p} \lambda_\tau N_\tau - \hbar\Omega\hat{J}_x + V. \quad (1)$$

The unperturbed Hamiltonian

$$\hat{H}_0 = \sum_i [h_{Nil}(i) + h_{add}(i)]$$

consists of the Nilsson Hamiltonian

$$h_{Nil} = \frac{p^2}{2m} + \frac{1}{2}m(\omega_1^2 x_1^2 + \omega_2^2 x_2^2 + \omega_3^2 x_3^2) - \\ - 2\kappa\hbar\omega_{00}\mathbf{l}\cdot\mathbf{s} - \kappa\mu\hbar\omega_{00}(\mathbf{l}^2 - \langle\mathbf{l}^2\rangle_N) \quad (2)$$

and the additional correction term [19]

$$h_{add} = \Omega m\omega_{00}\kappa\left\{2\left(r^2 s_x - x\mathbf{r}\cdot\mathbf{s}\right) + \\ + \mu\left[2r^2 - \frac{\hbar}{m\omega_{00}}\left(N + \frac{3}{2}\right)\right]l_x\right\}. \quad (3)$$

The correction term restores the local Galilean invariance broken in the rotating coordinate system and improves the description of the inertial properties in the Nilsson model (see Ref. [16]). The chemical potentials λ_τ (where $\tau = n, p$) are determined so as to give the correct mean particle numbers $\langle N_\tau\rangle$. Hereafter, $\langle\ldots\rangle$

denotes averaging over the mean-field vacuum (yrast) state at a given rotational frequency Ω. The two-body potential in Eq. (1) includes the monopole pairing, doubly stretched quadrupole–quadrupole and monopole–monopole interaction. Hamiltonian (1) has the inversion and signature symmetries. Using the generalized Bogoliubov transformation for quasiparticles and the variational principle (see the details in Ref. [20]), we obtain the Hartree–Bogoliubov (HB) equations for the positive-signature quasiparticle energies ε_i (protons or neutrons). The positive-signature $(r = +1)$ state is defined in accordance with the Bogoliubov transformation

$$\alpha_i^\dagger = \sum_k (\mathcal{U}_{ki} c_k^\dagger + \mathcal{V}_{\bar{k}i} c_{\bar{k}}), \quad e^{i\pi j_x} \alpha_i^\dagger e^{-i\pi j_x} = -i\alpha_i^\dagger,$$

where $|k\rangle$ denotes a single-particle state of a Goodman spherical basis (see Ref. [21]). By diagonalizing the Hamiltonian at the rotational frequency Ω, we obtain quasiparticle states with a good parity π and signature r. It suffices to solve the HB equations for the positive signature, because the negative-signature eigenvalues and eigenvectors are obtained from the positive ones as

$$(-\varepsilon_i, \mathcal{U}_i, \mathcal{V}_i) \rightarrow (\varepsilon_{\bar{i}}, \mathcal{V}_{\bar{i}}, \mathcal{U}_{\bar{i}}). \tag{4}$$

The index "$\bar{i}$" denotes the negative-signature $(r = -1)$ state $(e^{i\pi j_x} \alpha_{\bar{i}}^\dagger e^{-i\pi j_x} = i\alpha_{\bar{i}}^\dagger)$. For a given value of the rotational frequency Ω, the quasiparticle (HB) vacuum state is defined by $\alpha_i| \rangle = \alpha_{\bar{i}}| \rangle = 0$.

We solved the system of nonlinear HB equations for ^{156}Dy and ^{162}Yb on the mesh of deformation parameters β and γ defined by means of the oscillator frequencies in Eq. (2) as

$$\omega_i^2 = \omega_0^2 \left[1 - 2\beta \sqrt{\frac{5}{4\pi}} \cos\left(\gamma - \frac{2\pi}{3}i\right) \right], \tag{5}$$
$$i = 1, 2, 3 \quad \text{(or } x, y, z\text{)}.$$

The Nilsson–Strutinsky analysis of experimental data on high spins in ^{156}Dy [15] indicates that the positive-parity yrast sequence undergoes a transition from the prolate towards an oblate rotation. To compare our results with available experimental data on excited states [15], in comparison with our previous work [16], we extend the range of the values of γ from $\gamma = 60°$ (an oblate rotation around the y axis) to $\gamma = -60°$ (an oblate rotation around the x axis). At each rotational frequency and at each mesh point, we self-consistently calculate the total mean-field energy $E_{HB} = \langle \hat{H}_\Omega \rangle$. In the vicinity of the backbending, the solution becomes highly unstable. To avoid unwanted singularities for

certain values of Ω, we follow the phenomenological prescription [22]

$$\Delta_\tau(\Omega) =$$
$$= \begin{cases} \Delta_\tau(0) \left[1 - \frac{1}{2} \left(\frac{\Omega}{\Omega_c} \right)^2 \right], & \Omega < \Omega_c, \\ \frac{1}{2} \Delta_\tau(0) \left(\frac{\Omega_c}{\Omega} \right)^2, & \Omega > \Omega_c, \end{cases} \tag{6}$$

where Ω_c is the critical rotational frequency of the first band crossing.

It is well known that for a deformed harmonic oscillator, the quadrupole fields in doubly stretched coordinates [23] satisfy the stability conditions (cf. Ref. [24])

$$\langle \tilde{Q}_\mu \rangle = 0, \quad \mu = 0, 1, 2. \tag{7}$$

The tilde indicates that the quadrupole fields are expressed in terms of doubly stretched coordinates $\tilde{x}_i = (\omega_i/\omega_0) x_i$ and contain different combinations of the nonstretched quadrupole $Q_0 \propto (2z^2 - x^2 - y^2)$, $Q_2 \propto \sqrt{3}(x^2 - y^2)$ and monopole $M \propto r^2$ operators quantized along the z axis (cf. Ref. [23]). Condition (7) holds if the nuclear self-consistency condition

$$\omega_1^2 \langle x_1^2 \rangle = \omega_2^2 \langle x_2^2 \rangle = \omega_3^2 \langle x_3^2 \rangle \tag{8}$$

is satisfied in addition to the volume-preserving constraint. By virtue of condition (8), the doubly stretched residual interaction does not contribute to the mean-field results in the Hartree procedure. Enforcing the stability conditions (7) in the HB approximation, we search for the HB minimum for Hamiltonian (1) at a given rotational frequency. While the mean-field values of the quadrupole operators $\hat{Q}_0$ and $\hat{Q}_2$ are nonzero, the doubly stretched quadrupole moments $\langle \tilde{Q}_0 \rangle$ and $\langle \tilde{Q}_2 \rangle$ vanish (Fig. 1) for equilibrium deformations (Fig. 2).

The results of our calculations conform to the results of the Nilsson–Strutinsky shell-correction method (compare our Fig. 2 with Fig. 3c in Ref. [15]), although we obtain slightly different values for the equilibrium deformations. In the analysis in Ref. [15], the pairing correlations are missing. In addition, in the Nilsson–Strutinsky shell-correction method, the rigid-body moment of inertia simulates the inertial nuclear properties, which are different from the microscopic one, even in the high-spin region (see below). Moreover, the use of the Nilsson–Strutinsky results destroys the self-consistency between the mean-field calculations and the RPA analysis. Therefore, to maintain self-consistency between the mean-field approximation and
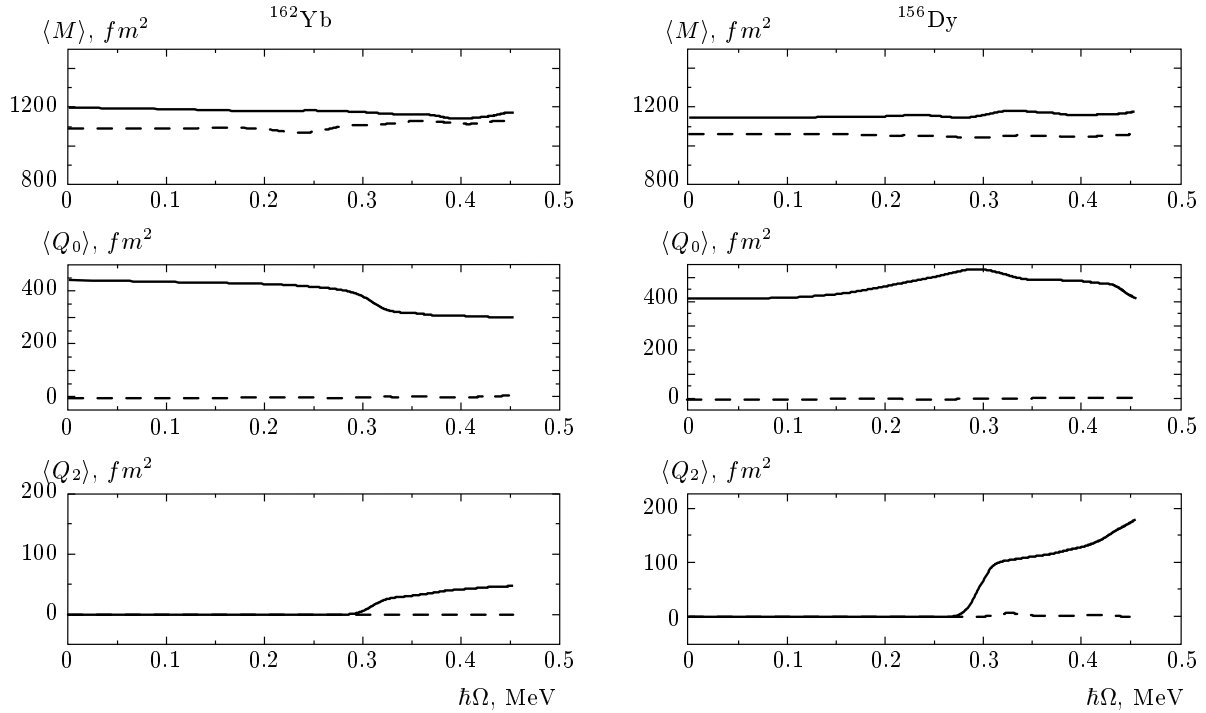
Fig. 1. The rotational behavior of the calculated monopole and quadrupole moments. The "doubly stretched" and standard values are connected by dashed and solid lines, respectively

the RPA as much as possible, we use the recipe described above.

The triaxiality of the mean field sets in at the critical rotational frequency Ω_c that triggers the backbending in the considered nuclei due to different mechanisms. We obtain $\hbar\Omega_c \approx 0.25$ MeV ($10\hbar \to 12\hbar$) and $\hbar\Omega_c \approx 0.3$ MeV ($14\hbar \to 16\hbar$) for ^{162}Yb and ^{156}Dy, respectively (see Fig. 2). The contribution of the additional term, Eq. (3), was crucial to achieve a good correspondence between the calculated and experimental values of the crossing frequency in each nucleus (see Ref. [16]).

In ^{156}Dy, we obtain that the γ-vibrational excitations ($K = 2$) of the positive signature tends to zero in the rotating frame at the transition point in close agreement with experimental data. At the transition point, there are two indistinguishable HB minima with different shapes: axially symmetric and strongly nonaxial. It is interesting to note that this behavior is symmetric with respect to the sign of the γ-deformation, although the difference between the HB energy minima for $\gamma = \pm 20°$ is about 0.8 MeV. The increase in the rotational frequency changes the axial shape to the nonaxial one with a negative γ-deformation ($\gamma \approx -20°$). The transition has all the features of a first-order sha-

pe–phase transition. In contrast to ^{156}Dy, the axially symmetric configuration in ^{162}Yb is replaced with the two-quasiparticle configuration with a small negative γ-deformation. There, the backbending occurs due to the rotational alignment of a neutron $i_{13/2}$ quasiparticle pair. The nonaxiality evolves quite smoothly, exhibiting the main features of a second-order shape–phase transition. The question arises as to how reliable our description is or how self-consistently our mean-field calculations are done.

One of the conclusive tests for the self-consistency of microscopic cranking calculations is the equivalence of the dynamic moment of inertia $\mathcal{J}_{HB}^{(2)}$ calculated in the mean-field approximation and the Thouless–Valatin moment of inertia $\mathcal{J}_{TV}$ calculated in the RPA. The equivalence certainly holds if a self-consistent mean-field minimum is found and spurious solutions are separated from the physical ones (see the results for an exactly solvable model in Ref. [25]). Our results (Fig. 3) demonstrate good consistency between the mean-field and the CRPA calculations. We emphasize that the inclusion of the correction term, Eq. (3), is crucial for achieving a good description of the inertial nuclear properties.
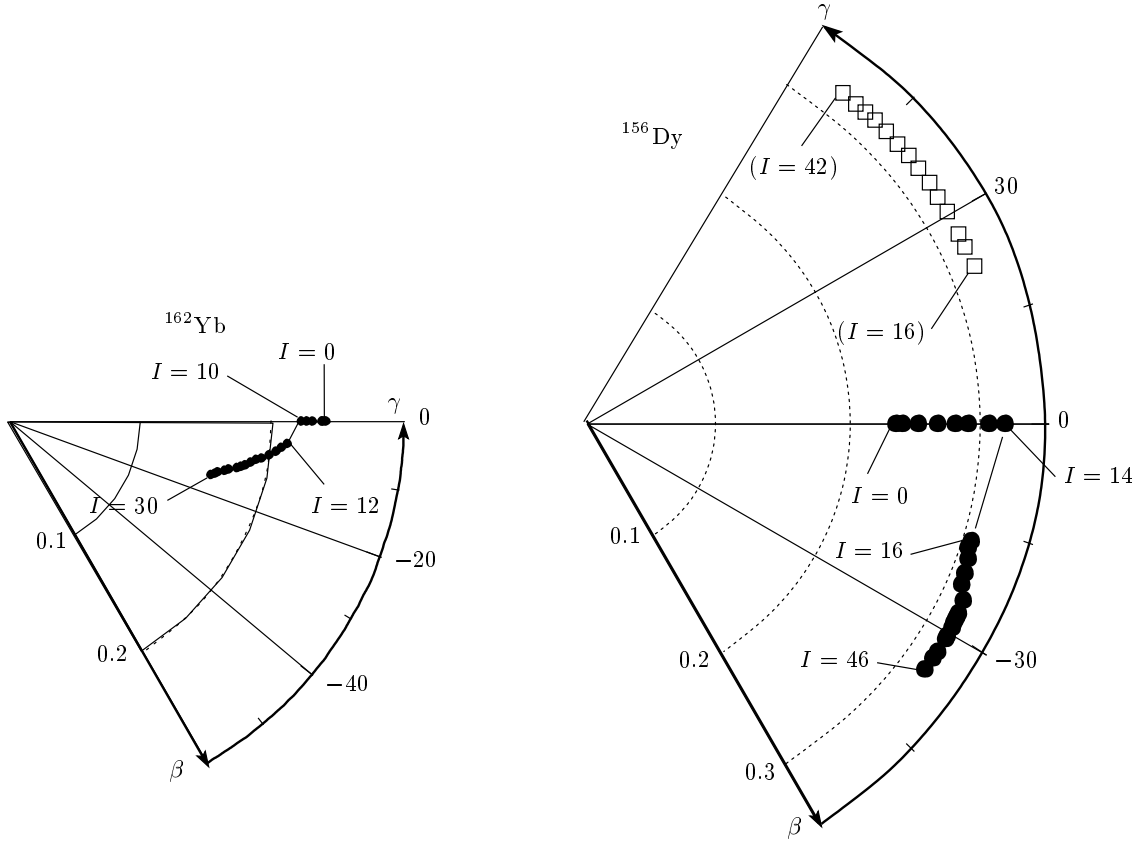
Fig. 2. Equilibrium deformations in the β–γ plane as a function of the angular momentum $I = \langle \hat{J}_x \rangle - 1/2$ (in units of $\hbar$). The equilibrium deformations for ^{156}Dy provide the lower mean-field energies in the region $-\pi/3 < \gamma < 0$ (filled circles) in comparison with those obtained in Ref. [16] (open squares). Both branches of the equilibrium deformations are obtained by enforcing condition (7). The maximum difference between the minimal HB energies at positive and negative equilibrium γ-values does not exceed 1 MeV for ^{156}Dy

2.2. Negative-signature excitations

To describe quantum oscillations around mean-field solutions, the boson-like operators

$$b^\dagger_{k\bar{l}} = \alpha^\dagger_k \alpha^\dagger_{\bar{l}}, \quad b^\dagger_{kl} = \alpha^\dagger_k \alpha^\dagger_l, \quad b^\dagger_{\bar{k}\bar{l}} = \alpha^\dagger_{\bar{k}} \alpha^\dagger_{\bar{l}}$$

are used. The first equality introduces a positive-signature boson, and the other two determine negative-signature ones. These two-quasiparticle operators are treated in the quasi-boson approximation (QBA) as elementary bosons, i.e., all commutators between them are approximated by their expectation values with the uncorrelated HB vacuum [26]. The corresponding commutation relations can be found in Ref. [20]. In this approximation, the positive- and negative-signature boson spaces are not mixed, because the corresponding operators commute and

$$\hat{H}_\Omega = \hat{H}_\Omega(r = +1) + \hat{H}_\Omega(r = -1).$$

The positive-signature term $\hat{H}_\Omega(r = +1)$ is analyzed in Ref. [16].

In the UR frame, the negative-signature RPA Hamiltonian has the form

$$\hat{H}_\Omega[r = -1] = \frac{1}{2} \sum_\mu E_\mu b^\dagger_\mu b_\mu - \frac{\chi}{2} \sum_{\mu_3 = 1,2} \tilde{Q}^{(-)2}_{\mu_3}, \quad (9)$$

where $E_\mu = \varepsilon_i + \varepsilon_j$ ($E_{\bar{i}\bar{j}} = \varepsilon_{\bar{i}} + \varepsilon_{\bar{j}}$) are two-quasiparticle energies. Hereafter, we use the following definitions: the index μ runs over ij, $\bar{i}\bar{j}$ and the index "μ_3" denotes the projection on the quantization axis z. The doubly stretched quadrupole operators

$$\tilde{Q}^{(-)}_1 = \xi \hat{Q}^{(-)}_1 \quad \left(\xi = \frac{\omega_x \omega_z}{\omega_0^2} \right),$$

$$\tilde{Q}^{(-)}_2 = \eta \hat{Q}^{(-)}_2 \quad \left(\eta = \frac{\omega_x \omega_y}{\omega_0^2} \right)$$

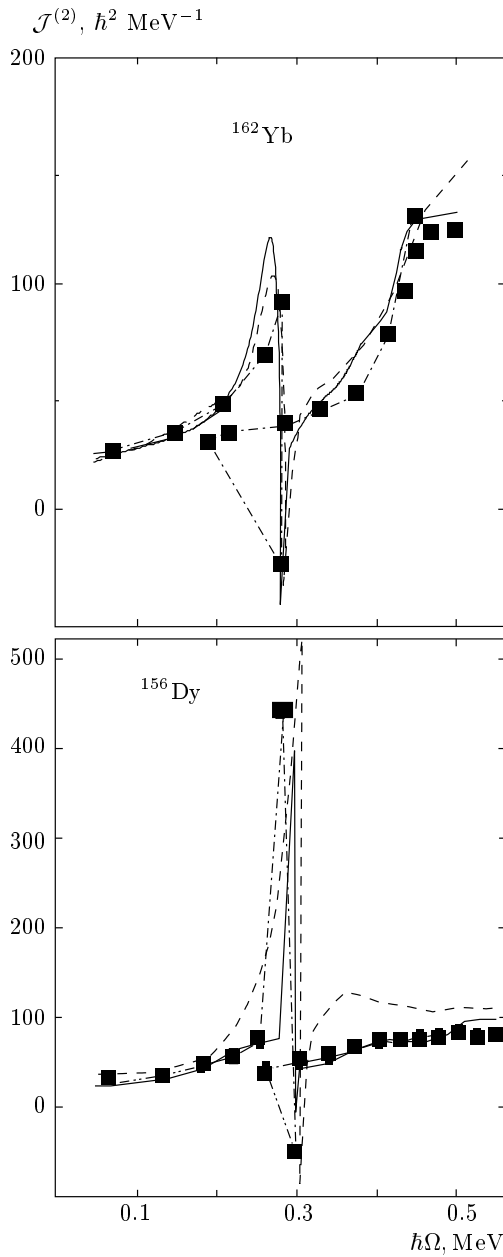are defined by means of the quadrupole operators $\hat{Q}^{(r)}_m$ ($m = 0, 1, 2$),

Fig. 3. The rotational dependence of the dynamic $\mathcal{J}_{HB}^{(2)} = -d^2 E_{HB}/d\Omega^2 = d\langle \hat{J}_x \rangle/d\Omega$ (the solid line) and the Thouless–Valatin $\mathcal{J}_{TV}$ moments of inertia (the dashed line). The experimental values $\mathcal{J}^{(2)} = 4/\Delta E_\gamma$ are denoted by filled squares connected by a dash-dotted line to guide the eye. ΔE_γ is the difference between two consecutive γ-transitions and E_γ is the γ-transition energy between two neighboring states that differ by two units of the angular momentum

$$\hat{Q}_m^{(r)} = \frac{i^{2+m+(r+3)/2}}{\sqrt{2(1+\delta_{m0})}} \times$$
$$\times \left(\hat{Q}_{2m} + (-1)^{(r+3)/2} \hat{Q}_{2-m} \right), \quad (10)$$

where $\hat{Q}_{\lambda m} = \hat{r}^\lambda Y_{\lambda m}$. We recall that the residual doubly stretched interaction does not distort the mean-field deformations found self-consistently for Hamiltonian (1).

The RPA Hamiltonian in (9) contains only the isoscalar part of the quadrupole interaction, because we wish to establish a connection between the microscopic approach and the phenomenological ARM to clearly see similarities and differences. Moreover, in the considered nuclei, the main contribution of the isovector quadrupole–quadrupole interaction is located in the energy region around 3 MeV and is responsible for M1 excitations [17]. We note, however, that the isovector part of the quadrupole interaction may be important for the analysis of wobbling excitations in odd–odd nuclei, having a different orientation of the neutron and proton single-particle high-j orbitals and strong $M1$-transitions along yrast and/or yrare states. The pairing interaction does not contribute to the boson Hamiltonian $\hat{H}_\Omega[r = -1]$ because it is of the positive signature. On the other hand, the matrix elements of the operators depend on the pairing interaction, which affects the RPA solutions.

The linear boson part of the doubly stretched operators has the form

$$\tilde{Q}_1^{(-)} = -\frac{1}{2} \sum_\mu \tilde{f}_{1\mu}(b_\mu^\dagger + b_\mu), \quad \tilde{f}_{1\mu} = \xi q_{1\mu}, \quad (11)$$

$$\tilde{Q}_2^{(-)} = -\frac{i}{2} \sum_\mu \tilde{f}_{2\mu}(b_\mu^\dagger - b_\mu), \quad \tilde{f}_{2\mu} = \eta q_{2\mu}, \quad (12)$$

where $q_{1\mu}$ and $q_{2\mu}$ are real matrix elements of the respective operators $\hat{Q}_1^{(-)}$ and $\hat{Q}_2^{(-)}$ (see the properties of matrix elements in Ref. [21]). We solve the RPA equations of motion

$$[\hat{H}_\Omega, \hat{P}_\nu] = i\,\omega_\nu\,\hat{X}_\nu, \quad [\hat{H}_\Omega, \hat{X}_\nu] = -i\,\omega_\nu\,\hat{P}_\nu,$$
$$[\hat{X}_\nu, \hat{P}_{\nu'}] = i\delta_{\nu\nu'}, \quad (13)$$

where $\hat{X}_\nu = \sum_\mu X_\mu^\nu(b_\mu^\dagger + b_\mu)$ and $\hat{P}_\nu = i\sum_\mu P_\mu^\nu(b_\mu^\dagger - b_\mu)$ are the collective coordinates and their conjugate momenta (hereafter, we set $\hbar = 1$ in all equations). The RPA eigenfunction

$$|\nu\rangle = \hat{O}_\nu^\dagger |\text{RPA}\rangle = \frac{1}{\sqrt{2}} \left(\hat{X}_\nu - i\hat{P}_\nu \right)|\text{RPA}\rangle =$$
$$= \sum_\mu (\psi_\mu^{(\nu)} b_\mu^\dagger - \phi_\mu^{(\nu)} b_\mu)|\text{RPA}\rangle \quad (14)$$

defines the amplitudes $\psi_\mu^{(\nu)}$ and $\phi_\mu^{(\nu)}$ by means of the generalized coordinate and momentum amplitudes. The ket vector $|\mathrm{RPA}\rangle$ denotes the RPA vacuum (yrast state) at the rotational frequency Ω. The solution of Eqs. (13) determines the generalized coordinate and momentum amplitudes,

$$
\begin{aligned}
X_\mu^\nu &= \chi \tilde{R}_1^\nu \frac{\omega_\nu \tilde{f}_{1\mu}}{E_\mu^2 - \omega_\nu^2} + \chi \tilde{R}_2^\nu \frac{E_\mu \tilde{f}_{2\mu}}{E_\mu^2 - \omega_\nu^2}, \\
P_\mu^\nu &= \chi \tilde{R}_1^\nu \frac{E_\mu \tilde{f}_{1\mu}}{E_\mu^2 - \omega_\nu^2} + \chi \tilde{R}_2^\nu \frac{\omega_\nu \tilde{f}_{2\mu}}{E_\mu^2 - \omega_\nu^2},
\end{aligned}
\tag{15}
$$

with unknown coefficients

$$
\begin{aligned}
\tilde{R}_1^\nu &= \sum_\mu \tilde{f}_{1\mu} P_\mu^\nu \equiv -\frac{1}{\sqrt{2}} \left[\hat{O}_\nu, \tilde{Q}_1^{(-)} \right], \\
\tilde{R}_2^\nu &= \sum_\mu \tilde{f}_{2\mu} X_\mu^\nu \equiv \frac{i}{\sqrt{2}} \left[\hat{O}_\nu, \tilde{Q}_2^{(-)} \right]
\end{aligned}
\tag{16}
$$

and eigenvalues ω_ν. To find the eigenvalues ω_ν, we transform system of equations (15) to the form

$$
\begin{aligned}
&\tilde{R}_1^\nu \left[D_{11}(\omega_\nu) - \frac{1}{\chi} \right] + \tilde{R}_2^\nu D_{12}(\omega_\nu) = 0, \\
&\tilde{R}_1^\nu D_{12}(\omega_\nu) + \tilde{R}_2^\nu \left[D_{22}(\omega_\nu) - \frac{1}{\chi} \right] = 0.
\end{aligned}
\tag{17}
$$

The condition

$$
F(\omega_\nu) = \det \left(\mathbf{D} - \frac{1}{\chi} \right) = 0
\tag{18}
$$

determines all negative-signature RPA solutions. The matrix elements

$$
D_{km}(\omega_\nu) = \sum_\mu \tilde{f}_{k,\mu} \frac{\tilde{f}_{m,\mu} C_\mu^{km}}{E_\mu^2 - \omega_\nu^2}
$$

involve the coefficients $C_\mu^{km} = \omega_\nu$ if $k \neq m$ and E_μ otherwise. Although the determinant has the dimension $n = 2$, we obtain a huge family of RPA solutions with different degrees of collectivity. Among collective solutions, there are solutions that correspond to shape fluctuations of the system. We note that the direction of the angular momentum is fixed in the UR frame.

3. THE WOBBLING MODE

3.1. Janssen–Mikhailov equation

We recall that in the RPA, the doubly stretched residual interaction restores the rotational symmetry broken in the mean-field approximation. Therefore, for

the cranking Hamiltonian, the conservation laws imply that the relations

$$
[\hat{H}_\Omega, \hat{J}_y \mp i\hat{J}_z] = \pm \Omega (\hat{J}_y \mp i\hat{J}_z)
\tag{19}
$$

hold in the RPA. This condition is equivalent to the condition of the existence of a negative-signature solution $\omega_\nu = \Omega$ created by the operator [27]

$$
\hat{\Gamma}^\dagger = \frac{\hat{J}_z + i\hat{J}_y}{\sqrt{2\langle \hat{J}_x \rangle}}, \quad \hat{\Gamma} = (\hat{\Gamma}^\dagger)^\dagger, \quad [\hat{\Gamma}, \hat{\Gamma}^\dagger] = 1.
\tag{20}
$$

The operator $\hat{\Gamma}^\dagger$ describes a collective rotational mode in the subspace of $\hat{H}_\Omega(r = -1)$ arising from the symmetries broken by the external rotational field (the cranking term). However, this is true only for a pure harmonic oscillator model [25]. Because the additional term h_{add} in Eq. (3) contains a term proportional to the $\hat{l}_x$ operator, conservation laws (19) are broken for Hamiltonian (1). Nevertheless, these laws can be satisfied in the RPA if the strength constant in Eq. (18) is changed in order to obtain the solution $\omega_\nu = \Omega$ [16]. To verify this fact, we calculated the RPA secular equation (18) for the mode $\omega_\nu = \Omega$, with and without the
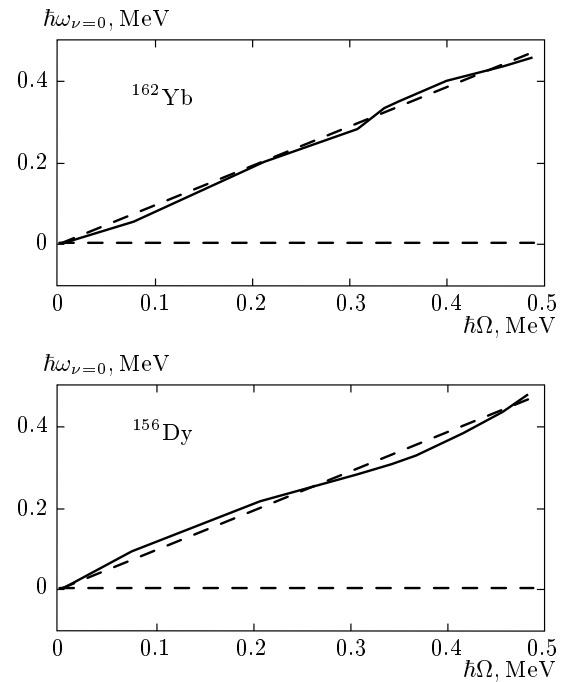

Fig. 4. Evolution of the negative-signature RPA solution $\omega_\nu = \Omega$ with (dashed line) and without (solid line) additional term (3) as a function of the rotational frequency, calculated at the equilibrium deformations (see Fig. 2). The straight dashed line parallel to the $\hbar\Omega$-axis is the yrast line

additional term h_{add}, for the same strength constant (see also Fig. 10 in Ref. [16]). The results evidently demonstrate that conservation law (19) is satisfied with a good accuracy (Fig. 4). In fact, due to a smallness of the term proportional to $\hat{l}_x$ in the additional term, the violation is almost negligible. Based on this fact, we use conservation laws (19) for Hamiltonian (9), which yield the equations

$$\Omega J_\mu^z + E_\mu J_\mu^y = \chi\xi A\tilde{f}_{1\mu}, \qquad (21)$$

$$\Omega J_\mu^y + E_\mu J_\mu^z = \chi\eta B\tilde{f}_{2\mu}. \qquad (22)$$

The parameters A and B defined by

$$\xi A = \langle[\tilde{Q}_1^{(-)}, iJ_y]\rangle = \sum_\mu \tilde{f}_{1\mu}J_\mu^y = \xi\langle Q_2+\sqrt{3}Q_0\rangle, \quad (23)$$

$$\eta B = \langle[\tilde{Q}_2^{(-)}, -iJ_z]\rangle = \sum_\mu \tilde{f}_{2\mu}J_\mu^z = 2\eta\langle Q_2\rangle \qquad (24)$$

are obtained with the aid of the commutator [28]

$$[\hat{J}_x \pm i\hat{J}_y, \hat{Q}_{\lambda m}] = \sqrt{\lambda(\lambda+1)-m(m\pm1)}\hat{Q}_{\lambda m\pm1}.$$

The above relations between the matrix elements, Eqs. (21) and (22), are a key point for the analysis of wobbling excitations at a nonzero γ-deformation, i.e., $\langle Q_2\rangle \neq 0$. Moreover, by virtue of the definitions of the phonon operator (Eqs. (14) and (15)) and the operator $\hat{\Gamma}$ (Eq. (20)), we can use Eqs. (21), (22), and (30) below to show that

$$[\hat{\Gamma}, \hat{O}_\nu] = [\hat{\Gamma}, \hat{O}_\nu^\dagger] = 0. \qquad (25)$$

Following the procedure described in Ref. [8], with the aid of Eqs. (21) and (22), we obtain the equation

$$(\omega_\nu^2 - \Omega^2)\Delta(\omega_\nu) = 0. \qquad (26)$$

The determinant $\Delta(\omega_\nu)$ corresponds to the system of equations

$$\begin{aligned} \omega_\nu S_y r_1^\nu - \Omega\mathcal{J}_{xy}r_2^\nu &= 0, \\ \Omega\mathcal{J}_{xz}r_1^\nu - \omega_\nu S_z r_2^\nu &= 0 \end{aligned} \qquad (27)$$

for the unknowns

$$r_1^\nu = \frac{\tilde{R}_1^\nu}{\xi A}, \quad r_2^\nu = \frac{\tilde{R}_2^\nu}{\eta B}. \qquad (28)$$

This system no longer has the solution $\omega_\nu = \Omega$. We introduce the notation

$$\begin{aligned} \mathcal{J}_{xy(z)} &= \mathcal{J}_x - \mathcal{J}_{y(z)} - \omega_\nu^2 S/\Omega, \\ S_{y,z} &= \mathcal{J}_{y,z} + \Omega S, \end{aligned} \qquad (29)$$

where $\mathcal{J}_x = \langle\hat{J}_x\rangle/\Omega$ is the kinematic moment of inertia,

$$S = \sum_\mu \frac{J_\mu^y J_\mu^z}{E_\mu^2 - \omega_\nu^2},$$

and

$$\mathcal{J}_{y,z} = \sum_\mu \frac{E_\mu(J_\mu^{y,z})^2}{E_\mu^2 - \omega_\nu^2}.$$

From system (27), we obtain the relation between the unknowns r_1^ν and r_2^ν as

$$\frac{r_1^\nu}{r_2^\nu} = \frac{\Omega\mathcal{J}_{xy}}{\omega_\nu S_y} = \frac{\omega_\nu S_z}{\Omega\mathcal{J}_{xz}}, \qquad (30)$$

which is helpful in our analysis below.

The condition $\Delta(\omega_\nu) = 0$ leads to the Janssen–Mikhailov equation [8]

$$\Delta(\omega_\nu) = \omega_\nu^2 - {} \\ - \Omega^2 \frac{[\mathcal{J}_x-\mathcal{J}_y-\omega_\nu^2 S/\Omega][\mathcal{J}_x-\mathcal{J}_z-\omega_\nu^2 S/\Omega]}{[\mathcal{J}_y+\Omega S][\mathcal{J}_z+\Omega S]} = 0, \quad (31)$$

which determines all vibrational modes of negative signature excluding the solution $\omega_\nu = \Omega$. We stress that the solution of this equation alone is meaningless. While Eq. (31) is independent of the strength constant, the violation of conditions (21) and (22) via an arbitrary variation of the γ-deformation or pairing gap destroys the link between the systems of Eqs. (17) and (27). As a result, the redundant mode cannot be removed from Eq. (18) and it is impossible to obtain Eq. (31). Providing the wobbling solution, this equation has a different form than the Bohr–Mottelson classical equation, however. Below, we present a simple derivation of the microscopic analog of the latter equation.

3.2. Marshalek moments of inertia

Relations (30) are equivalent to

$$\frac{r_1^\nu S_y}{r_2^\nu S_z} = \frac{\Omega\mathcal{J}_{xy}}{\omega_\nu S_z} = \frac{\omega_\nu S_y}{\Omega\mathcal{J}_{xz}} \qquad (32)$$

and can be associated with the system of equations

$$\begin{aligned} \omega_\nu S_z a - \Omega\mathcal{J}_{xy}b &= 0, \\ \Omega\mathcal{J}_{xz}a - \omega_\nu S_y b &= 0 \end{aligned} \qquad (33)$$

for the unknowns $a = r_1^\nu S_y$ and $b = r_2^\nu S_z$. Using definitions (29), we rearrange this system to the form

$$\omega_\nu\left(\mathcal{J}_z+\omega_\nu S\frac{b}{a}\right)a-\Omega\left(\mathcal{J}_x-\mathcal{J}_y-\omega_\nu S\frac{a}{b}\right)b = 0, \\ \Omega\left(\mathcal{J}_x-\mathcal{J}_z-\omega_\nu S\frac{b}{a}\right)a-\omega_\nu\left(\mathcal{J}_y+\omega_\nu S\frac{a}{b}\right)b = 0. \qquad (34)$$

Using (32), we define the effective moments of inertia in the UR frame as

$$
\begin{aligned}
\mathcal{J}_2^{eff} &= \mathcal{J}_y + \omega_\nu S \frac{a}{b} = \mathcal{J}_y + \Omega S \frac{\mathcal{J}_{xy}}{S_z}, \\
\mathcal{J}_3^{eff} &= \mathcal{J}_z + \omega_\nu S \frac{b}{a} = \mathcal{J}_z + \Omega S \frac{\mathcal{J}_{xz}}{S_y},
\end{aligned}
\tag{35}
$$

which depend on the RPA frequency. Definitions (35) are the same as those obtained by Marshalek in the time-dependent HB approach but in the principal-axis (PA) frame [9]. The determinant for nonzero solutions of system (34) yields a nonlinear equation similar to the classical expression for the wobbling mode [1],

$$
\omega_{\nu=w} = \Omega \sqrt{\frac{[\mathcal{J}_x - \mathcal{J}_2^{eff}][\mathcal{J}_x - \mathcal{J}_3^{eff}]}{\mathcal{J}_2^{eff} \mathcal{J}_3^{eff}}}, \tag{36}
$$

with the microscopically defined moments of inertia. Equation (36) was obtained by Marshalek in the PA frame from the equations for the amplitudes of the angular-frequency time oscillations. In the UR (time-independent) frame, we obtain this equation with much less effort. It is evident that for the rotation around the x axis, the wobbling excitations with different collectivity can be found from Eq. (36) if the condition

$$
\mathcal{J}_x > \mathcal{J}_2^{eff}, \mathcal{J}_3^{eff} \quad (\text{or} \quad \mathcal{J}_x < \mathcal{J}_2^{eff}, \mathcal{J}_3^{eff}) \tag{37}
$$

is satisfied. It can be expected that for the RPA solutions different from the wobbling mode, this condition should not hold. We note that Eq. (18) contains the solutions of Eq. (36) but not vice versa, because constraint (37) is valid in the latter case but is not required in the former. We obtain quite a remarkable correspondence between the experimental and calculated values for the kinematic moment of inertia for both nuclei (see top panels in Fig. 5). We also trace the evolution of the irrotational fluid moment of inertia and a rigid-body moment of inertia (cf. Ref. [26]) as functions of the equilibrium deformations (see Fig. 2). The irrotational fluid moment of inertia reproduces neither the rotational dependence nor the absolute values of the experimental one as functions of the rotational frequency. The rigid-body values provide the asymptotic limit of fast rotation without pairing. Evidently, the difference between the rigid-body and the calculated kinematic moments of inertia in both nuclei decreases as the rotational frequency increases, although it remains visible at high spins. At very fast rotation, $\hbar\Omega > 0.45$ MeV, the pairing correlations are reduced due to multiple alignments, and the difference is therefore moderated.
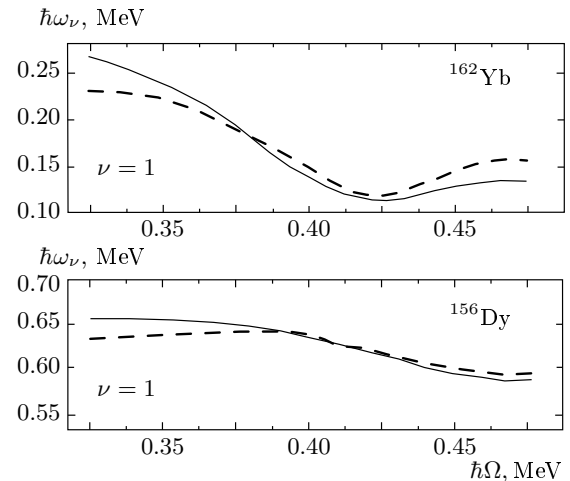

Fig. 6. The rotational dependence of the RPA solutions obtained with the aid of Eq. (18) (solid line) and Eq. (36) (dashed line). The RPA solutions obtained with the aid of Eq. (18) satisfy condition (37)

The Marshalek moments of inertia in Eq. (35), calculated for the first RPA solution of Eq. (18), signal the appearance of the wobbling mode after a shape–phase transition in ^{162}Yb and ^{156}Dy (see Fig. 5, bottom panels). As stressed above, the separation of the redundant mode is an essential point for the RPA wobbling theory that secures a reliable analysis of the RPA modes. Additionally, to ensure the self-consistency of our RPA calculations, we compare the solutions that may be associated with wobbling excitations from different RPA Eqs. (18) and (36). We recall that Eq. (18) depends on the strength constant χ and contains different RPA solutions including the redundant mode, while this dependence is removed from Eq. (36). Evidently, if the redundant mode were not removed from Eq. (18) by our choice of the strength constants, conditions (21) and (22) would be broken. As a result, the consistency between Eqs. (18) and (36) would be broken as well and these equations would provide different solutions. A nice agreement between the roots of Eqs. (18) and (36) (Fig. 6) confirms the viability and validity of our approach. Below, we formulate specific criteria for identifying collective wobbling excitations among RPA solutions of Eq. (18).

3.3. Criteria for wobbling excitations

Using Eqs. (34) and (35), we can define the unknown variables $r_1^{\nu=w} = a/S_y$, $r_2^{\nu=w} = b/S_z$ (which determine the wobbling mode) such that
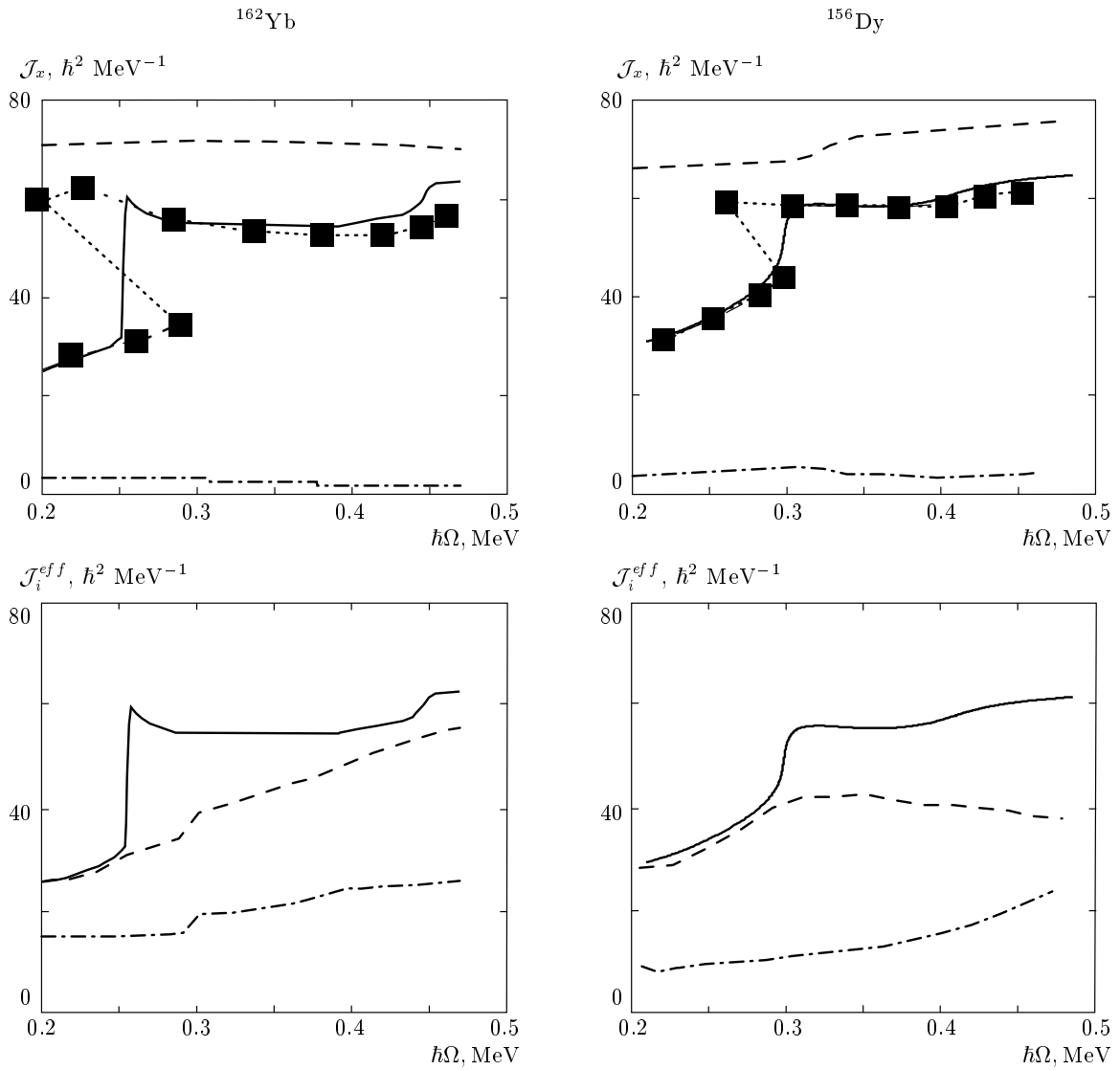
^{162}Yb

^{156}Dy

Fig. 5. Top panels: the kinematic $\mathcal{J}_x = \langle \hat{J}_x \rangle / \Omega$ (solid line), the rigid-body $\mathcal{J}_1^{(rig)} = \frac{2}{5} m A R^2 \left(1 - \sqrt{\frac{5}{4\pi}} \beta \cos(\gamma - \frac{2\pi}{3}) \right)$ (dashed line), and the hydrodinamical $\mathcal{J}_1^{(irr)} = \frac{3}{2\pi} m A R^2 \beta^2 \sin^2 \left(\gamma - \frac{2\pi}{3} \right)$ (dash-dotted line) moments of inertia are compared with the experimental values (filled squares). Experimental values $\mathcal{J}_x = I/\Omega$ are connected by dotted lines to guide the eye ($\hbar\Omega = E_\gamma/2$). Bottom panels: the rotational dependence of the kinematic moment of inertia (solid line), Marshalek moments of inertia $\mathcal{J}_2^{eff}$ (dashed line) and $\mathcal{J}_3^{eff}$ (dash-dotted line) for the first RPA solution $\nu = 1$ obtained from Eq. (18)

$$\frac{r_1^w}{r_2^w} = \frac{S_z}{S_y} \frac{a}{b} = \frac{S_z}{S_y} \frac{\Omega(\mathcal{J}_x - \mathcal{J}_2^{eff})}{\omega_w \mathcal{J}_3^{eff}} =$$

$$= \frac{S_z}{S_y} \frac{\omega_w \mathcal{J}_2^{eff}}{\Omega(\mathcal{J}_x - \mathcal{J}_3^{eff})} = \sqrt{\frac{W_2}{W_3}} \frac{S_z}{S_y} \frac{\mathcal{J}_2^{eff}}{\mathcal{J}_3^{eff}}. \quad (38)$$

Here, we used that the dispersion equation for the wobbling mode, Eq. (36), can be expressed as $\omega_w = \langle \hat{J}_x \rangle \sqrt{W_2 W_3}$, where

$$W_2 = \left(\frac{1}{\mathcal{J}_2^{eff}} - \frac{1}{\mathcal{J}_x} \right), \quad W_3 = \left(\frac{1}{\mathcal{J}_3^{eff}} - \frac{1}{\mathcal{J}_x} \right). \quad (39)$$

With the aid of Eqs. (35) and definition (29), it is easy to show that $S_z \mathcal{J}_2^{eff} / S_y \mathcal{J}_3^{eff} \equiv 1$. Therefore,

$$\frac{r_1^w}{r_2^w} = \sqrt{\frac{W_2}{W_3}}. \quad (40)$$

By means of the inverse transformation

$$b_\mu^\dagger = \sqrt{2} \sum_\nu X_\mu^\nu (\hat{O}_\nu^\dagger - \hat{O}_\nu) + P_\mu^\nu (\hat{O}_\nu^\dagger + \hat{O}_\nu), \quad (41)$$

we can express the operators $\tilde{Q}_{1,2}^{(-)}$ (see Eqs. (11), (12), and (16)) in terms of the phonon operators:

$$\tilde{Q}_1^{(-)} = -\sqrt{2} \sum_\nu \tilde{R}_1^\nu (\hat{O}_\nu^\dagger + \hat{O}_\nu), \quad (42)$$

$$\tilde{Q}_2^{(-)} = -i\sqrt{2} \sum_\nu \tilde{R}_2^\nu (\hat{O}_\nu^\dagger - \hat{O}_\nu). \quad (43)$$

We use that the components of the quadrupole tensor commute, i.e., the condition

$$\left[\tilde{Q}_1^{(-)}, \tilde{Q}_2^{(-)} \right] = 4i \sum_{\nu=all} \tilde{R}_1^\nu \tilde{R}_2^\nu =$$
$$= 2 \sum_{\nu=all} \left[\hat{D}_\nu, \tilde{Q}_1^{(-)} \right] \left[\hat{D}_\nu, \tilde{Q}_2^{(-)} \right] = 0 \quad (44)$$

holds. Here, we use the notation $\hat{D}_{\nu=\Omega} \equiv \hat{\Gamma}$ and $\hat{D}_{\nu\neq\Omega} \equiv \hat{O}_\nu$ for other vibrational modes. Taking definitions (16) and (28) into account (also see Eqs. (20), (23), and (24)), we obtain the exact definitions for the unknowns $r_{1,2}^\Omega$ associated with the redundant mode:

$$r_1^\Omega = \frac{\tilde{R}_1^{\nu=\Omega}}{\xi A} = -\frac{1}{\xi A \sqrt{2}} \left[\hat{\Gamma}, \tilde{Q}_1^{(-)} \right] = -\frac{1}{2\sqrt{\langle \hat{J}_x \rangle}},$$
$$r_2^\Omega = \frac{\tilde{R}_2^{\nu=\Omega}}{\eta B} = \frac{i}{\eta B \sqrt{2}} \left[\hat{\Gamma}, \tilde{Q}_2^{(-)} \right] = \frac{1}{2\sqrt{\langle \hat{J}_x \rangle}}. \quad (45)$$

This result allows expressing the sum in Eq. (44) as

$$\sum_{\nu \neq w, \Omega} r_1^\nu r_2^\nu + r_1^w r_2^w = -r_1^\Omega r_2^\Omega = \frac{1}{4\langle \hat{J}_x \rangle}. \quad (46)$$

We suppose that the sum in the left-hand side of Eq. (46), defined by all physical solutions excluding the wobbling one, is zero due to a mutual cancellation of different terms. As a result, we obtain the equation for the unknowns $r_{1,2}^w$. Solving this equation with the aid of Eq. (40), we obtain

$$r_1^w = \frac{1}{2\sqrt{\langle \hat{J}_x \rangle}} \left(\frac{W_2}{W_3} \right)^{1/4},$$
$$r_2^w = \frac{1}{2\sqrt{\langle \hat{J}_x \rangle}} \left(\frac{W_3}{W_2} \right)^{1/4}. \quad (47)$$

These expressions are similar to those of the wobbling mode in the Bohr–Mottelson model (see the Appendix, Eqs. (A.14)), although the quantities $W_{2,3}$ are

determined by the Marshalek moments of inertia and $\langle \hat{J}_x \rangle \approx I + 1/2$ (the factor $1/2$ occurs due to the RPA contribution of the redundant mode, see the discussion in Ref. [29]). Similar expressions were obtained in Ref. [7] in the PA frame (with the quantization condition $\langle \hat{J}_x \rangle = I$ and some additional phases).

To identify the wobbling mode among the solutions of Eq. (18), it is convenient to transform Eq. (44) to the form

$$\sum_{\nu=all} c_\nu = 0, \quad c_\nu = 4\langle \hat{J}_x \rangle \frac{\tilde{R}_1^\nu}{\xi A} \frac{\tilde{R}_2^\nu}{\eta B}. \quad (48)$$

It follows from Eqs. (45) and (47) that

$$c_{\nu=\Omega} = -1, \quad c_{\nu=w} = 1. \quad (49)$$

Thus, if we solve only the system of the RPA equations for the quadrupole operators, Eq. (18), condition (49) allows identifying the redundant and the wobbling modes.

3.4. Analysis of experimental data

The experimental level sequences for all the currently observed rotational bands in ^{162}Yb and ^{156}Dy are taken from Ref. [14]. All rotational states are classified by the quantum number α, which is equivalent to our signature r. The positive-signature states ($r = +1$) correspond to $\alpha = 0$ because the quantum number α leads to selection rules for the total angular momentum $I = \alpha + 2n$, $n = 0, \pm 1, \pm 2, \ldots$ (cf. Ref. [30]). In particular, in even–even nuclei, the yrast band characterized by the positive-signature quantum number $r = +1$ ($\alpha = 0$) consists of even spins only. The negative-signature states ($r = -1$) correspond to $\alpha = 1$ and are associated with odd-spin states in even–even nuclei. All considered bands are of positive parity $\pi = +$.

The redundant mode and four lowest RPA solutions of Eq. (18) as functions of the rotational frequency are shown in Figs. 7a and 8a. We recall that these solutions are found at different equilibrium deformations (see Fig. 2). Indeed, in both nuclei, criterion (49) uniquely determines the redundant and the wobbling modes. In Figs. 7b and 8b, the redundant mode is manifested as a straight line, while the corresponding coefficient c_Ω is always -1 (Figs. 7c and 8c). The rotational mode is clearly separated from the vibrational modes. We note that the solutions that are different from rotational and wobbling modes contribute to the sum in Eq. (46) with zero weight, as was proposed above.

To compare our results with the available experimental data on low-lying excited states near the yrast
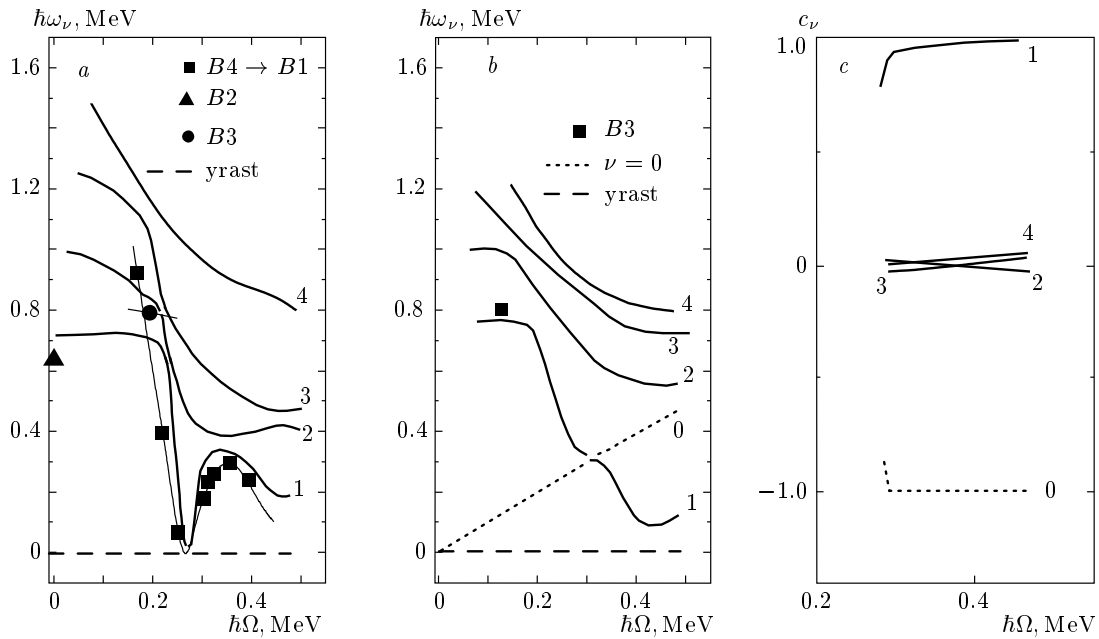
Fig. 7. The results for ^{162}Yb. *a*) The rotational dependence of the positive-signature RPA solutions with even spins ($\pi = +, \alpha = 0$). The number denotes the RPA solution number: 1 is the first ($\nu = 1$) RPA solution, etc. Different symbols display the experimental data associated with $B1$, $B2$, ... bands (the band labels are taken in accordance with the definitions given in Ref. [14]). *b*) The rotational dependence of the negative-signature RPA solutions with odd spins ($\pi = +$, $\alpha = 1$). The redundant mode $\omega_\nu = \Omega$ is denoted by "0" and is displayed by the dotted line. *c*) The rotational dependence of the coefficients $c_\nu \sim \tilde{R}_1^\nu \tilde{R}_2^\nu$ (see Eq. (48)) determined by solutions of Eq. (18)
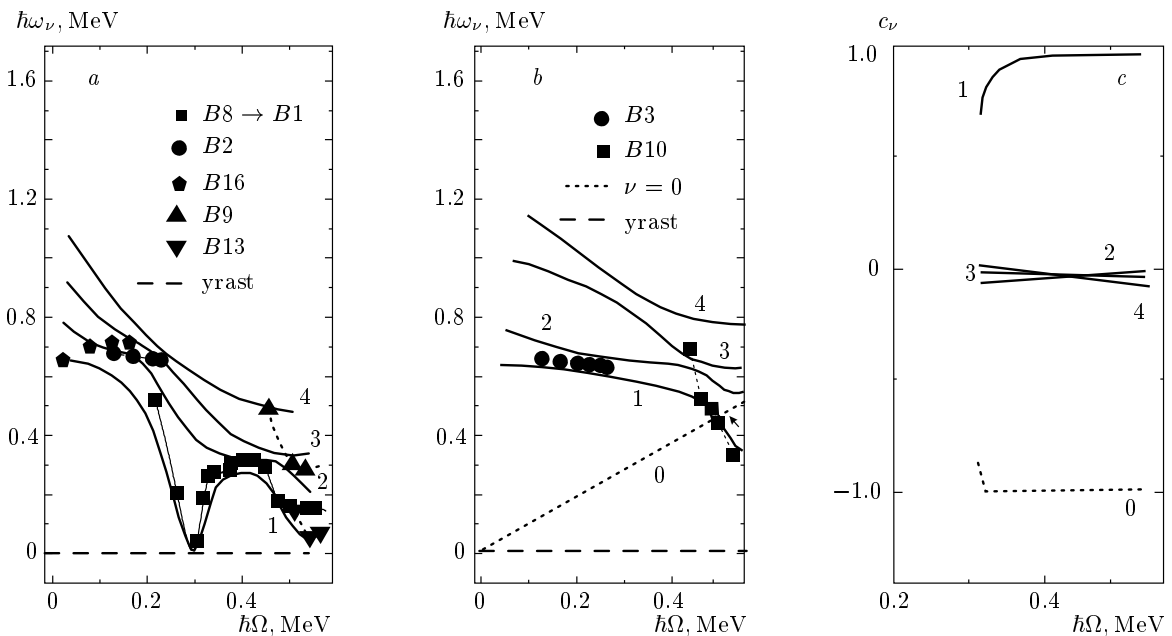

Fig. 8. The same as in Fig. 7 for ^{156}Dy

line [14], we construct experimental Routhians for each rotational band ν ($\nu = $ yrast, $\beta, \gamma, \dots$):

$$R_\nu(\Omega) = E_\nu(\Omega) - \hbar\Omega I_\nu(\Omega),$$

$$\Omega(I) = [E_\nu(I+1) - E_\nu(I-1)]/2,$$

and define the experimental excitation energy in the rotating frame as $\hbar\omega_\nu^{exp} = R_\nu(\Omega) - R_{yr}(\Omega)$ [31]. In ^{162}Yb, only one negative-signature γ-vibrational state is known. The first RPA solution ($\nu = 1$) is a negative-signature γ-vibrational mode (with odd spins) up to $\hbar\Omega \approx 0.28$ MeV. With an increase in the rotational frequency, it is transformed into the wobbling mode at $\hbar\Omega \approx 0.32$ MeV (according to criterion (49)). The other solutions ($\nu = 2, 3, 4$) contribute to the sum in Eq. (46) with zero weight. Our results for the $\nu = 1$ solution may be used as a guideline for possible experiments on identification of the wobbling excitations near the yrast line. Although the positive-signature states have been discussed in Ref. [16], for completeness of our analysis we compare RPA results for the positive signature with an updated database in [14]. According to our analysis, the first RPA solution of positive signature may be identified with β-excitations at small rotation $\hbar\Omega \leq 0.2$ MeV. With an increase in the rotational frequency, a strong mixing between γ-excitation (the second RPA solution at low spins) and β-excitation occurs. At $\hbar\Omega \geq 0.2$ MeV, the first RPA solution of positive signature is determined by a single two-quasiparticle neutron configuration (see the discussion and Table 1 in Ref. [16]).

In ^{156}Dy, the first ($\nu = 1$) positive-signature RPA solution carries a large portion of quasiparticle states with $K = 2$. Because the quantum number K is reliable at small angular momenta, we associate the first positive-signature RPA solution with the γ-vibrational mode. Rotation leads to a strong mixing between the first and the second RPA solutions. With an increase in the rotational frequency, the first solutions is separated from the second one, while the latter strongly interacts with the third RPA solution. At $\hbar\Omega \approx 0.3$ MeV, there is a crossing between the $B1$ (yrast) band and the $B8$ (excited) band, which becomes the yrast one after the transition point. The first positive-signature RPA solution describes this transition with a good accuracy: the RPA mode vanishes at $\hbar\Omega \approx 0.3$ MeV. We recall that according to our analysis in [16], precisely this vibrational mode is responsible for the backbending phenomenon in this nucleus.

The first negative-signature RPA solution in ^{156}Dy can be associated with the negative-signature γ-vibrational mode with odd spins. After the transition

from the axial to nonaxial rotation, at $\hbar\Omega \approx 0.3$ MeV, according to criterion (49), the first negative-signature RPA solution describes the wobbling excitations. The mode preserves its features with the increase in the rotational frequency up to $\hbar\Omega \approx 0.55$ MeV. There is a good agreement (see Fig. 8) between this one-phonon band and the experimental Routhian of band $B10$ (or the $(+, 1)_1$ band according to Ref. [15]). Based on this, we propose to consider the $B10$ band as the wobbling band in the range 0.45 MeV$< \hbar\Omega < 0.55$ MeV ($33\hbar \leq I \leq 39\hbar$ for this band). We note that the $B10$ band contains the states with $31\hbar - 53\hbar$. However, our conclusion is reliable only for states with $I = 33\hbar - 39\hbar$ (or up to $\hbar\Omega < 0.55$ MeV). At $\hbar\Omega \approx 0.55$ MeV, a crossing of the negative-parity and negative-signature (positive simplex) $B6$ band with the yrast band $B8$ is observed. At $\hbar\Omega > 0.55$ MeV (or for $I > 39\hbar$ for the $B10$ band), the onset of octupole deformation in the yrast states may be expected. The octupole deformation is beyond the scope of our model, based on the quadrupole deformed mean field, and this feature will be discussed elsewhere.

The proposed criterion in Eq. (49) is necessary but not sufficient for concluding that we have found a solution related to the wobbling excitations. It is brought about by the formal equivalence between the classical (Eq. (A.3) in the Appendix) and the microscopic (Eq. (36)) equations for the wobbling mode. Our solution is determined in the UR frame, where the fluctuations of the angular momentum are absent (they are responsible for the wobbling mode in the PA frame). To identify the wobbling mode, we also have to specify the relation between electromagnetic transitions in the Bohr–Mottelson model defined in the PA systems and our model defined in the UR frame.

3.5. Electromagnetic transitions

Transition probabilities for the $X\lambda$ transition $|I\nu\rangle \to |I'\nu'\rangle$ between two high-spin states are given by

$$B(X\lambda; I\nu \to I'\nu') \approx$$
$$\approx (I\,I\,\lambda\,\mu_1\,|\,I'\,I')^2 |\langle\nu'|\hat{\mathcal{M}}(X\lambda; \mu_1 = I' - I)|\nu\rangle|^2. \quad (50)$$

In the high-spin limit ($I \gg \lambda$, $I' \gg \lambda$), the transition from a one-phonon state into the yrast-line state takes the form [32]

$$B(X\lambda; I\nu \to I'yr)) \approx$$
$$\approx \left|\langle\mathrm{RPA}|\left[\hat{\mathcal{M}}^{(1)}(X\lambda; \mu_1 = I'-I), \hat{O}_\nu^\dagger\right]|\mathrm{RPA}\rangle\right|^2, \quad (51)$$

where $\hat{\mathcal{M}}^{(1)}(X\lambda\mu_1)$ is the linear boson part of the corresponding transition operator of type X, multipolarity λ, and the projection μ_1 onto the rotation axis x in the UR frame. The commutator in (51) can be easily expressed in terms of phonon amplitudes $\psi_\mu^{(\nu)}$ and $\phi_\mu^{(\nu)}$ (see Eq. (14)). With the aid of the transformation from x- to z-axis quantization [32],

$$\hat{\mathcal{M}}(X\lambda\mu_1) = \sum_{\mu_3} \mathcal{D}^\lambda_{\mu_3\mu_1}\left(0, \frac{\pi}{2}, 0\right) \hat{\mathcal{M}}(X\lambda\mu_3), \quad (52)$$

and definitions (16) and (28), and taking into account that the relation

$$\langle\nu|\hat{M}^{(E)}_{2\mu_3=0,2}|\nu\rangle = \langle\hat{M}^{(E)}_{2\mu_3=0,2}\rangle$$

holds in the first RPA order, we obtain

$$B(E2; I\nu \to I \pm 1yr) = \left|\left\langle\left[\hat{M}^{(E)}_{2\mu_1=\pm 1}, \hat{O}_\nu^\dagger\right]\right\rangle\right|^2 =$$
$$= \left|\frac{i}{\sqrt{2}\eta}\left[\tilde{O}_2^{(-)(E)}, \hat{O}_\nu^\dagger\right] \mp \frac{1}{\sqrt{2}\xi}\left[\tilde{O}_1^{(-)(E)}, \hat{O}_\nu^\dagger\right]\right|^2, \quad (53)$$

where $\hat{M}^{(E)} = (eZ/A)\hat{M}$. By Eqs. (16) and (47), the above expression yields the definition of the quadrupole transitions from the one-phonon wobbling state to the yrast states,

$$B(E2; Iw \to I \pm 1yr) =$$
$$= \frac{1}{4\langle\hat{J}_x\rangle}\left|\left(\frac{W_2}{W_3}\right)^{1/4} A^{(E)} \mp \left(\frac{W_3}{W_2}\right)^{1/4} B^{(E)}\right|^2, \quad (54)$$

which is similar to Eq. (A.13) in the Appendix. Thus, we provide a complete microscopic definition of the wobbling excitations in accordance with the criteria suggested by Bohr and Mottelson for the rigid rotor [1]. We note a clear difference between the microscopic and the rigid rotor models: the microscopic moments of inertia, Eqs. (35), should be calculated for the RPA solutions of Eq. (18) that must satisfy condition (49).

For intraband transitions, we have (see Eq. (43) in [16])

$$B(E2; I\nu \to I - 2\nu) = \left|\langle\nu|\hat{\mathcal{M}}(E2; \nu_1 = 2)|\nu\rangle\right|^2 =$$
$$= \frac{1}{8}\left|\sqrt{3}\langle\hat{Q}_0^{(E)}\rangle - \langle\hat{Q}_2^{(E)}\rangle\right|^2. \quad (55)$$

For illustrative purposes, to give a rough idea on the major trend of quadrupole transitions, we use the relations from the pairing-plus-quadrupole model (cf. Ref. [30]):

$$m\omega_0^2\beta\cos\gamma = \chi\langle Q_0\rangle, \quad m\omega_0^2\beta\sin\gamma = -\chi\langle Q_2\rangle.$$

From these relations and the definition of the quadrupole isoscalar strength,

$$\chi = \frac{4\pi m\omega_0^2}{5\langle r^2\rangle} \approx \frac{4\pi m\omega_0^2}{3AR^2}, \quad R \approx 1.2A^{1/3} \text{ fm},$$

we obtain

$$B(E2; In_w = 1 \to I \pm 1 \text{ yr}) = \Theta\frac{\beta^2}{\langle\hat{J}_x\rangle} \times$$
$$\times \left[\left(\frac{W_2}{W_3}\right)^{1/4}\sin\left(\frac{\pi}{3} - \gamma\right) \pm \left(\frac{W_3}{W_2}\right)^{1/4}\sin\gamma\right]^2, \quad (56)$$

where $\Theta = (9/16\pi^2)e^2 Z^2 R^4$. For $W_{2,3} > 0$, Eq. (56) yields selection rules for the quadrupole transitions from the one-phonon wobbling band to the yrast one:
$-60° < \gamma < 0$:

$$B(E2; In_w \to I - 1 \text{ yr}) >$$
$$> B(E2; In_w \to I + 1 \text{ yr}), \quad (57a)$$

$0 < \gamma < 60°$:

$$B(E2; In_w \to I + 1 \text{ yr}) >$$
$$> B(E2; In_w \to I - 1 \text{ yr}). \quad (57b)$$

For the intraband transitions, we obtain

$$B(E2; In_w \to I - 2n_w) = \frac{1}{2}\Theta\beta^2\cos^2\left(\frac{\pi}{6} - \gamma\right). \quad (58)$$

It follows from Eq. (58) that for the transitions along the yrast line ($n_w = 0$), the onset of the positive (negative) values of the γ-deformation leads to an increase (decrease) in the transition probability along the yrast line. Experimental values of $B(E2, I\nu \to I' \text{ yr})$ are deduced from the half life of the yrast states [14] using the standard, long-wave-limit expressions [26]

$$B(E2, i \to f) = \frac{P(i \to f)}{1.223 \cdot 10^9 E_\gamma^5}, \quad e^2 \cdot \text{fm}^4.$$

Here, the transition energy E_γ is in megaelectronvolts and the absolute transition probability $P(i \to f) = \ln 2/T(i \to f)$ is related to the half life $T(i \to f)$ (in seconds). In comparing our results with experimental data, we take the Clebsch–Gordan coefficient into account (see Eq. (50)) up to $I \leq 10\hbar$. For $I > 10\hbar$, the asymptotic value for the Clebsch–Gordan coefficient, which is 1, is used. We note that in the vicinity of the backbending, the mean-field description becomes less reliable (cf. Ref. [33]). While the cranking approach should be complemented with a projection technique in the backbending region due
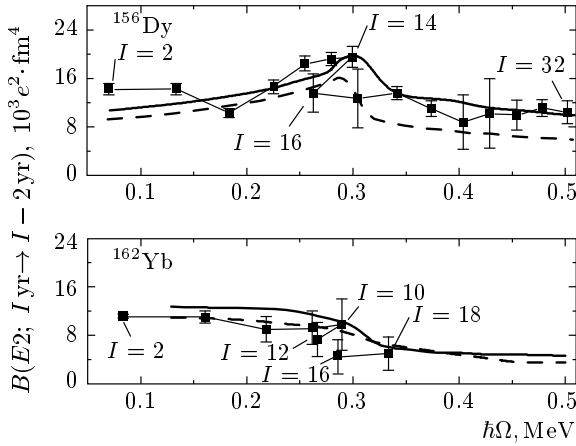
Fig. 9. Reduced transition probabilities $B(E2; I\,\mathrm{yr} \to$ $\to I - 2\,\mathrm{yr})$ along the yrast line. Experimental data (filled squares) are connected with a thin line to guide the eye. The results of calculations based on Eqs. (58) and (55) are connected by dashed and solid lines, respectively

to large fluctuations of the angular momentum (cf. Ref. [26]), its validity becomes much better at high spins. Evidently, the larger the rotational frequency, the better the predictive quality of the CRPA because it is based on the cranking approach aimed for the high-spin physics [30].

Experimental data for the quadrupole transitions along the yrast line are compared with the results of calculations (a) by means of Eq. (55) and (b) by means of Eq. (58) (Fig. 9). In calculations (a), we use the mean-field values for the quadrupole operators. Calculations (a) evidently manifest the backbending effect obtained for the moments of inertia (see Fig. 5) at $\hbar\Omega_c \approx 0.25$ MeV and $\hbar\Omega_c = 0.3$ MeV for ^{162}Yb and ^{156}Dy, respectively. Thus, the use of the self-consistent expectation values $\langle \hat{Q}_m^{(E)} \rangle$ is crucial in order to reproduce the experimental behavior of the yrast band decay. Calculations (b) (Eq. (58)) reproduce the experimental data with less accuracy, while providing the major trend of the transitions with the sign of γ-deformation. The agreement between the calculated and experimental values of intraband $B(E2)$ transitions along the yrast line is especially good after the transition point.

At small rotational frequency, in both nuclei, transitions probabilities from the first positive- and negative-signature RPA solutions are much weaker in comparison with the quadrupole transitions along the yrast line (see Fig. 9 and top panels in Figs. 10 and 11). At $\hbar\Omega \approx 0.05$ MeV, the transition strengths for the first positive ($r = +1$) and negative ($r = -1$) RPA

solutions are approximately 330 $e^2 \cdot$ fm^4 for ^{162}Yb and 500 $e^2 \cdot$ fm^4 for ^{156}Dy with small differences between different transitions due to Clebsch–Gordan coefficients. We obtain a good correspondence between the shape evolution and selection rules (57) for both nuclei (see top panels in Figs. 10 and 11 and Fig. 2). Transition probabilities (53) are calculated using the $\psi_\mu^{(\nu)}$ and $\phi_\mu^{(\nu)}$ phonon amplitudes expressed in terms of the coordinate and momentum amplitudes (see Eqs. (14), (15), (16), and (28)). We compare these results for the first negative-signature RPA solution (which is associated with a wobbling mode) with the results obtained by means of the Marshalek moments of inertia (see Eqs. (35), (39), and (54)). Evidently, if the "spurious" solution (the redundant mode) is not removed from Eq. (18), it contributes to the variables (28). These variables cannot obey condition (30) in this case. As a result, orthogonality condition (25) is broken and Eqs. (53) and (54) for the transitions should produce completely different results. A good agreement between both calculations (see the right top panels in Figs. 10 and 11) is the most valuable proof of the validity of our approach. The observed negligible differences are due to the approximate fulfillment of conservation laws (19), caused by the presence of additional term (3) (see Fig. 4).

According to our analysis, a transition from the axially deformed to nonaxial shapes with the negative γ-deformation in ^{162}Yb occurs at $\hbar\Omega \approx 0.25$ MeV (see Fig. 2 and the discussion in Ref. [16]). At $\hbar\Omega \geq 0.28$ MeV, the excited band of the negative signature, created by the first RPA solution, changes the decay properties. The negative values of γ-deformation produce the dominance of the interband quadrupole transitions from the one-phonon state to the yrast ones with a lower spin ($\Delta I = 1$, the case in Eq. (57a)).

Similar results are obtained in ^{156}Dy for the lowest negative-signature excited band created by the first RPA solution. At low angular momenta ($\hbar\Omega \leq 0.3$ MeV), this band populates the yrast states with $I' = I \pm 1$ with approximately equal probabilities (I is the angular momentum of the excited state). At $\hbar\Omega \approx 0.3$ MeV, a shape–phase transition occurs, which leads to the triaxial shapes with the negative γ-deformation. In turn, the excited band created by the first RPA solution decays stronger on the yrast states with angular momenta $I' = I - 1$ ($\Delta I = 1$, the case in Eq. (57a)), starting from $\hbar\Omega \geq 0.32$ MeV.

It follows from the above analysis of the electric quadrupole transitions that there is no need to know the definition of the wobbling phonon operator in the
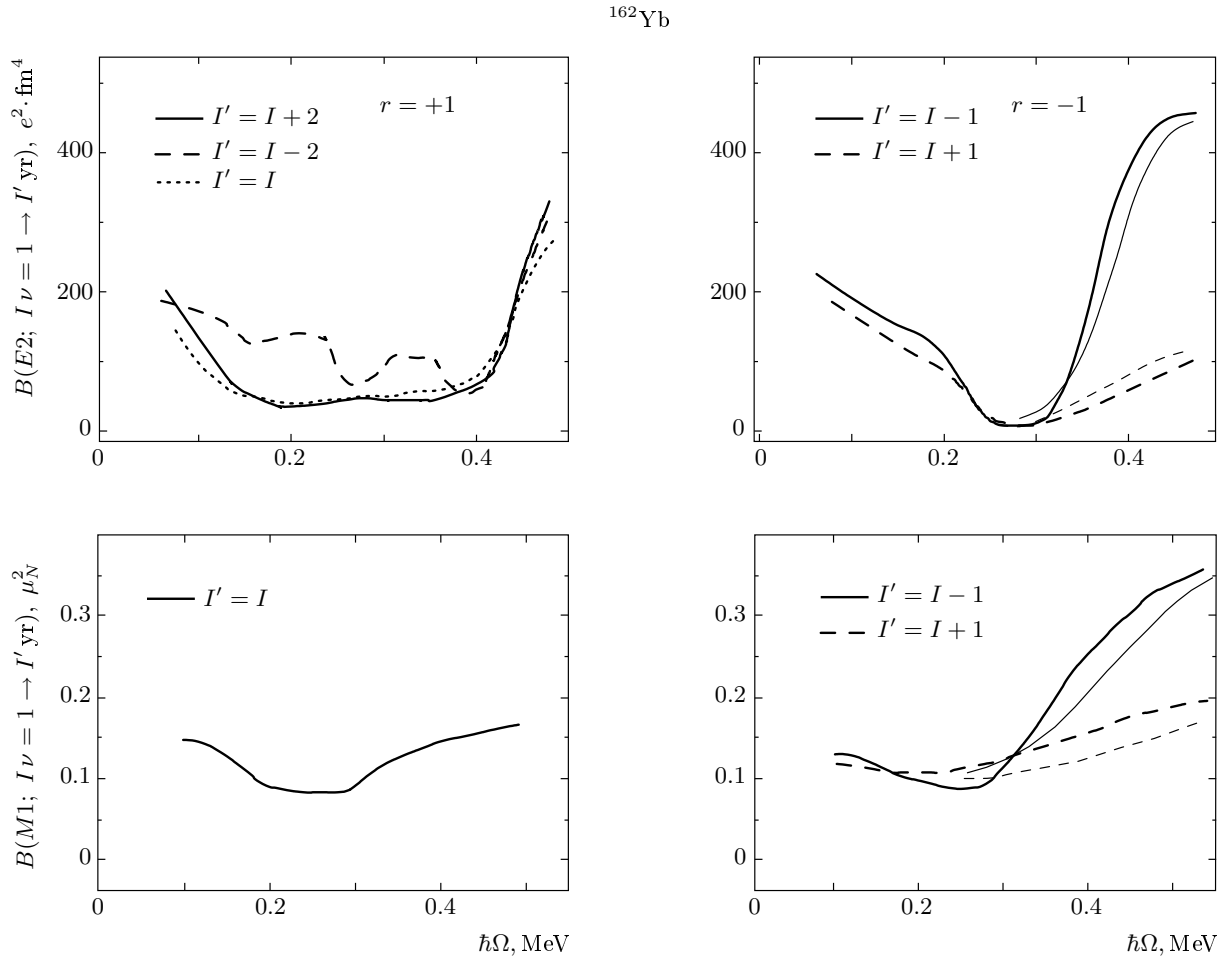
$$^{162}\text{Yb}$$

Fig. 10. The electric $B(E2)$- (top) and the magnetic $B(M1)$- (bottom) reduced probabilities of transition from the one-phonon bands to the yrast band. The positive- (negative) signature phonon band is described by the first $r = +1$ ($r = -1$) RPA solution. We observe a strong dominance of the $B(E2)$- and $B(M1)$-transitions from the wobbling states ($r = -1$) with spin I to the yrast states with spin $I' = I - 1$, starting from the rotational frequency $\hbar\Omega > 0.28$ MeV. The transitions calculated using the $\psi_\mu^{(\nu=1)}$ and $\phi_\mu^{(\nu=1)}$ phonon amplitudes are connected by thick lines. In the right panels, the results obtained using Eqs. (54) and (65) (with the aid of the variables $W_{2,3}$, Eq. (39)) are connected by thin lines, starting from the rotational frequency $\hbar\Omega \approx 0.3$ MeV. This point is associated in our analysis with the appearance of wobbling excitations

UR frame. Indeed, in this frame, the direction of the angular momentum is fixed and fluctuations of the angular momentum are absent. But there is a vibrational mode related to shape fluctuations that carries one unit of angular momentum. In the PA frame, according to the analysis of Bohr and Mottelson, the system shape is fixed, while the angular momentum fluctuates around the rotation axis that coincides with one of the principal axes of the inertia tensor. Evidently, the result for the transition probabilities in the laboratory frame must be independent of the choice of the reference frame.

To prove the equivalence of both results for the elec-

tric quadrupole transitions, we use the Bohr–Mottelson definition of the wobbling phonon operator, Eq. (A.5),

$$\hat{Q}_w^\dagger = \frac{i}{\sqrt{2\langle\hat{J}_x\rangle}} \times$$

$$\times \left[(\hat{I}_2)_{PA} \left(\frac{W_2}{W_3} \right)^{1/4} + (i\hat{I}_3)_{PA} \left(\frac{W_3}{W_2} \right)^{1/4} \right]. \quad (59)$$

Here, the quantities $W_{2,3}$ are determined by the Marshalek moments of inertia, Eqs. (39). In the PA frame, we must use transformation (A.12) in order to calculate the transition probability and commutation rela-
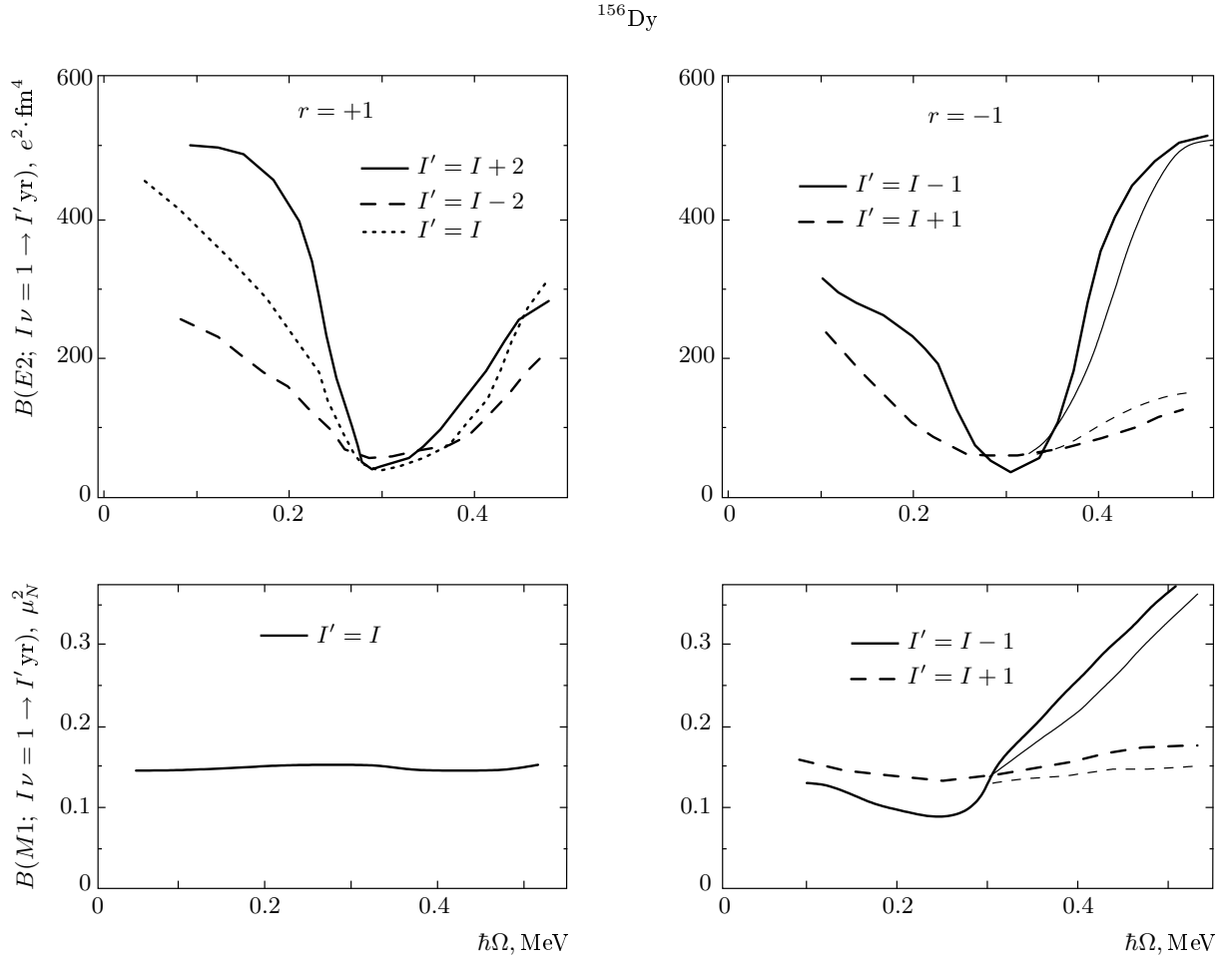
^{156}Dy

Fig. 11. Similar to Fig. 10. A strong dominance of the $B(E2)$- and $B(M1)$-transitions from the wobbling states ($r = -1$) with spin I to the yrast states with spin $I' = I - 1$ starting from the rotational frequency $\hbar\Omega \geq 0.3$ MeV can be observed

tions (A.2). This transformation and definition (59) yield the expression

$$B(E2; Iw \to I \pm 1\,\mathrm{yr}) = \left| \left\langle \left[\hat{M}^{(E)}_{2\mu_1 = \pm 1}, \hat{O}^{\dagger}_w \right] \right\rangle \right|^2 =$$

$$= \frac{1}{4\langle \hat{J}_x \rangle} \left| \left(\frac{W_2}{W_3} \right)^{1/4} A^{(E)} \mp \left(\frac{W_3}{W_2} \right)^{1/4} B^{(E)} \right|^2, \quad (60)$$

which is indeed the same as Eq. (54), obtained in the UR frame. We use this fact below to understand major features of the magnetic transitions from the wobbling band.

In the CRPA approach, the magnetic transitions are defined as

$$B(M1; Iv \to I \pm 1\,\mathrm{yr}) \approx \left| \left\langle \left[\hat{M}^{(M)}_{1\mu_1 = \pm 1}, \hat{O}^{\dagger}_\nu \right] \right\rangle \right|^2. \quad (61)$$

With the aid of the transformation from the x-axis to the z-axis quantization in Eq. (52), we obtain

$$B(M1; Iv \to I \pm 1\,\mathrm{yr}) \approx$$

$$\approx \frac{1}{2} \left| i \left[\hat{M}^{(M)}_{1\nu_3 = 1}, \hat{O}^{\dagger}_\nu \right] \mp \left[\hat{M}^{(M)}_{1\nu_3 = 0}, \hat{O}^{\dagger}_\nu \right] \right|^2. \quad (62)$$

The linear bosonic term of the magnetic operator has the form (see also Ref. [21])

$$\hat{M}^{(M)}_{1\nu_3 = 0,1} = \mu_N \sqrt{3} \left(\frac{1}{2} g_s^{(eff)} \hat{S}_{01\nu_3} + g_l^{(eff)} \hat{L}_{01\nu_3} \right) =$$

$$= \frac{i^{\nu_3 + 2}}{2} \sum_\mu \Lambda^{(\nu_3)}_\mu \left[b^{\dagger}_\mu + (-1)^{\nu_3} b_\mu \right], \quad (63)$$

where μ_N is the nucleon magneton, $g_s^{(eff)}$ and $g_l^{(eff)}$ are the spin and orbital effective gyromagnetic ratios, respectively, and the quasiparticle matrix elements $\Lambda^{(\nu_3)}_\mu$ are real. Taking the definition of the phonon operator in Eq. (14) into account, we express the magnetic

transition with the aid of generalized coordinate and momentum amplitudes (15) as

$$B(M1; I\nu \to I \pm 1\,\mathrm{yr}) \approx$$

$$\approx \left| \sum_\mu \Lambda_\mu^{(1)} X_\mu^\nu \mp \sum_\mu \Lambda_\mu^{(0)} P_\mu^\nu \right|^2 . \quad (64)$$

Our results evidently demonstrate the dominance of $B(M1; I\,n_W \to I - 1\,\mathrm{yr})$ (see the right bottom panels in Figs. 10 and 11) for both nuclei. To understand this result, we define the magnetic transitions using the Marshalek moments of inertia. With the aid of definition (59), transformation (A.12), and commutation relations

$$[\hat{I}_1 \pm i\hat{I}_2, \hat{M}_{\lambda m}] = \sqrt{\lambda(\lambda + 1) - m(m \mp 1)}\, \hat{M}_{\lambda m \mp 1}$$

for the PA frame [34], we obtain from Eq. (61) that

$$B(M1; I\,\nu \to I \pm 1\,\mathrm{yr}) \approx \left| \langle \hat{M}_{1\nu_3=1}^{(M)}[r = +1] \rangle \right|^2 \times$$

$$\times \frac{1}{4\langle \hat{J}_x \rangle} \frac{\left(\sqrt{W_3} \mp \sqrt{W_2} \right)^2}{\sqrt{W_2 W_3}}. \quad (65)$$

Although the expression for the magnetic transitions in Eq. (65) is similar to the one of the Bohr–Mottelson model, we stress that the moments of inertia are defined self-consistently within the CRPA approach. We note that the dipole magnetic moment $\langle \hat{M}_{1\nu_3=1}^{(M)}[+] \rangle$ increases quite drastically if a nucleus undergoes backbending (see the discussion about the $M1$ strength in Ref. [17]). Keeping in mind that $W_{2,3} > 0$ for the wobbling states, we have

$$B(M1; I n_W \to I - 1\,\mathrm{yr}) >$$

$$> B(M1; I\,n_W \to I + 1\,\mathrm{yr}). \quad (66)$$

Therefore, the tendency observed in the microscopic calculations with the aid of the phonon amplitudes is understood in terms of rules (66). Independently of the sign of the γ-deformation of rotating nonaxial nuclei, these rules determine the dominance of $\Delta I = 1\hbar$ magnetic transitions from the wobbling to the yrast states.

4. SUMMARY

We presented a transparent, self-consistent derivation of the basic equations for the wobbling excitations in the UR (time-independent) frame, which determine the energy spectrum and electromagnetic properties of these states in even–even nuclei. We obtained the same

expressions (35) for the effective moments of inertia as those obtained by Marshalek in the time-dependent Hartree–Bogoliubov approach in the PA frame [9]. We established a one-to-one correspondence between the main characteristics of the wobbling excitations in the Bohr–Mottelson model and those derived within the CRPA approach. We note, however, that the CRPA breaks down at the transition point when Δ_p or Δ_n vanishes [32]. We have avoided this problem by means of the phenomenological prescription for the rotational dependence of the pairing gap. A good agreement between the dynamic moment of inertia calculated in the mean-field approximation and the Thouless–Valatin moment of inertia calculated in the RPA supports the consistency of our mean-field calculations (see Fig. 3). In contrast to the standard RPA calculations, where the residual strength constants are fixed for all values of Ω (see, e.g., [7, 12, 13]), we determined the strength constants for each value of Ω by the requirement of the validity of conservation laws. This allows overcoming the instability of RPA calculations at the transition region, for the excitations at least. In principle, projection methods may be used in the transition region in order to calculate transition matrix elements. Although the amplitudes $\phi_\mu^{(\nu)}$ (see Eq. (14)) are larger for the RPA modes in the transition region than in other regions, the relation $|\phi_\mu^{(\nu)}| < |\psi_\mu^{(\nu)}|$ is still valid. The CRPA also becomes quite effective at high spins, after the transition point, when the pairing correlations still persist.

It follows from our analysis that an excited band can be regarded as the wobbling one if the magnetic transitions from this band into the yrast one satisfy condition (66). We note that these rules are independent of the γ-deformation sign. In contrast, the collective electric quadrupole transitions from this band to the yrast one must satisfy staggering rules (57) depending on the γ-deformation sign. We predict that the lowest excited negative-signature and positive-parity band in ^{162}Yb (which is a natural prolongation of the odd angular momentum part of the γ-band) transforms to the wobbling band at $\hbar\Omega > 0.3$ MeV. We found that strong $E2$ transitions from this band populate the yrast states, with the branching ratio

$$B(E2; Iw \to I - 1\,\mathrm{yr})/B(E2; Iw \to I + 1\,\mathrm{yr}) > 1.$$

Such behavior is brought about by the onset of nonaxial nuclear shapes with the negative sign of γ-deformation after the backbending. According to our definition of γ-deformation, with an increase in the rotational frequency, the system is driving to a noncollective oblate rotation (around the x axis). This trend is

confirmed by a good agreement between the results for the quadrupole transitions along the yrast line and available experimental data (see Fig. 9). A similar transition also occurs in ^{156}Dy after the backbending, at $\hbar\Omega > 0.3$ MeV. In this nucleus, we found that the lowest negative-signature and positive-parity band represents a natural prolongation of the γ-band with odd spins, observed at small angular momenta up to $\hbar\Omega \approx 0.3$ MeV. At rotational frequencies $\hbar\Omega > 0.3$ MeV, this band transforms to the wobbling band. A good agreement between our results and experimental Routhians allows concluding that the experimental states associated with the $(+, 1)_1$ band in Ref. [15] are wobbling excitations at the rotational frequency values 0.45 MeV$< \hbar\Omega <$ 0.55 MeV. These states satisfy all the requirements that are specific for the wobbling excitations of nonaxially deformed rotating nuclei, with the negative γ-deformation.

It turns out that strongly deformed triaxial shapes produce relatively high-lying vibrational states, associated with a wobbling mode (the case of ^{156}Dy). In contrast, a soft shape–phase transition from the axially deformed to nonaxial shapes provides the low-lying wobbling excitations (the case of ^{162}Yb). Further detailed studies are required to shed light on the interplay between different shape–phase transitions and their manifestations by means of vibrational states at high spins. Evidently, it is quite desirable to obtain new experimental data on electromagnetic decay properties of these states in order to reach a final conclusion about our prediction and, consequently, on the validity of the CRPA analysis.

APPENDIX

Asymmetric rotor model

In this appendix, we review the basic features of the wobbling excitations in the rotor model [1] in order to compare it with the microscopic model discussed in Sec. 3. In addition to well-known results, we provide a novel analysis of magnetic properties of the wobbling states.

In the high-spin limit $I \gg 1$, the rotor Hamiltonian has the form (see Ref. [1])

$$\hat{H} = \hat{H}_0 + \frac{\hbar^2}{2\mathcal{J}_1}(\hat{I})^2_{PA} + \hat{H}_{wobb}, \qquad (A.1)$$

$$[\hat{I}_i, \hat{I}_j]_{PA} = -i\varepsilon_{ijk}(\hat{I}_k)_{PA}, \qquad (A.2)$$

where $(\hat{I}_i)^2_{PA}$ and $\mathcal{J}_i$ are the angular momentum and principal moment of inertia components in the rotating, principal-axis (PA) coordinate system. It is assumed that the yrast band is generated by rotation around the x axis $I \approx I_1 = K$. Small oscillations of the angular momentum create wobbling excitations described by the term

$$\hat{H}_{wobbl} = \hbar\omega_w \left(\hat{Q}^\dagger_{wobb}\hat{Q}_{wobb} + \frac{1}{2} \right),$$
$$\hbar\omega_w = \hbar^2 I \sqrt{W_2 W_3}, \qquad (A.3)$$

where

$$W_2 = \frac{1}{\mathcal{J}_2} - \frac{1}{\mathcal{J}_1}, \quad W_3 = \frac{1}{\mathcal{J}_3} - \frac{1}{\mathcal{J}_1}. \qquad (A.4)$$

The wobbling (excited) state at spin I is created by the wobbling phonon

$$\hat{O}^\dagger_{wobb} = xB^\dagger - yB \Leftrightarrow B^\dagger = x\hat{O}^\dagger_{wobb} + y\hat{O}_{wobb} \qquad (A.5)$$

with

$$B^\dagger = \frac{i}{\sqrt{2I}}(\hat{I}_2 + i\hat{I}_3)_{PA}, \quad B = (B^\dagger)^\dagger, \qquad (A.6)$$

$$x = \frac{\sqrt{W_3} + \sqrt{W_2}}{2}(W_2 W_3)^{-1/4}, \qquad (A.7)$$

$$y = \frac{\sqrt{W_2} - \sqrt{W_3}}{2}(W_2 W_3)^{-1/4}, \qquad (A.8)$$

and the normalization condition $x^2 - y^2 = 1$. It follows from Eq. (A.3) that the diagonalization of $\hat{H}_{wobb}$ requires $W_2 > 0$, $W_3 > 0$, and $\mathcal{J}_1 > \mathcal{J}_2 > \mathcal{J}_3$.

At $I \approx I_1 \gg 0$, the eigenfunction of Hamiltonian (A.1) is given by the Wigner $\mathcal{D}$-function times the intrinsic eigenfunction defined by the wobbling quantum number $|n_w\rangle = (Q^\dagger_{wobb})^{n_w}|0\rangle$. The variable

$$n_w = \langle IK|B^\dagger B|IK\rangle \approx I - I_1 = I - K \qquad (A.9)$$

is defined with respect to the state $|IK = (I_1)_{PA}\rangle \equiv \equiv |n_w\rangle$ such that

$$B^\dagger|IK\rangle = \sqrt{n_w + 1}|IK - 1\rangle = \sqrt{n_w + 1}|n_w + 1\rangle,$$

$$|0\rangle = |IK = I\rangle.$$

The transition probability for the operator of the type X and multipolarity λ,

$$B(X\lambda; I\nu K_\nu \to I'\nu' K'_\nu) =$$
$$= \frac{1}{2I+1}|\langle I'K'_\nu\nu'||\hat{\mathcal{M}}(X\lambda)||IK_\nu\nu\rangle|^2, \quad (A.10)$$

is defined by the reduced matrix element

$$\langle I'K'n'_w||\hat{\mathcal{M}}(X\lambda)||IKn_w\rangle = \sqrt{2I+1} \times$$
$$\times \sum_{\nu_1=-\lambda}^{\lambda} \langle n'_w|(IK\lambda\nu_1|I'K')\hat{\mathcal{M}}(X\lambda\nu_1 = I'-I)|n_w\rangle. \quad (A.11)$$

We note that the eigenmodes of the Hamiltonian $\hat{H}_0$ do not change the projection K onto the first PA axis. But if the wobbling mode is excited with $|n'_w - n_w| \neq 0$, the projection K changes and the corresponding Clebsch–Gordan coefficients in Eq. (A.11) can be expressed in terms of the $B^\dagger$ and B operators (see Sec. 4.5c in Ref. [1]).

Using this procedure for the Clebsch–Gordan coefficients, a relation between multipole operators in the PA frame with the x- and z-quantization axis, and definition (10),

$$\hat{\mathcal{M}}(X\lambda\mu_1) = \sum_{\mu_3} \mathcal{D}^\lambda_{\mu_1\mu_3}\left(0, \frac{\pi}{2}, 0\right)\hat{\mathcal{M}}(X\lambda\mu_3), \quad (A.12)$$

we obtain the interband $E2$ transitions between the one-phonon wobbling band ($n_w = 1$) and the yrast band ($n_w = 0$) as

$$B(E2; In_w \to I \pm 1 \text{ yr}) =$$
$$= |\varrho_1 A^{(E)} \mp \varrho_2 B^{(E)}|^2, \quad (A.13)$$

where the variables $A^{(E)}$ and $B^{(E)}$ are defined by Eqs. (23) and (24), $\hat{Q}_m^{(E)} \equiv e\dfrac{Z}{A}\hat{Q}_m$, and

$$\varrho_1 = \frac{1}{\sqrt{2I}}\left(\frac{W_2}{W_3}\right)^{1/4}, \quad \varrho_2 = \frac{1}{\sqrt{2I}}\left(\frac{W_3}{W_2}\right)^{1/4}. \quad (A.14)$$

For intraband transitions, we have

$$B(E2; In_w \to I - 2 n_w) =$$
$$= \frac{1}{8}\left|\sqrt{3}\langle\hat{Q}_0^{(E)}\rangle - \langle\hat{Q}_2^{(E)}\rangle\right|^2, \quad (A.15)$$

where we use that

$$\langle\hat{\mathcal{M}}(E2, \nu_1 = \pm 1)\rangle = 0,$$
$$\langle\hat{\mathcal{M}}(E2, \nu_1 = 2)\rangle = \langle\hat{\mathcal{M}}(E2, \nu_1 = -2)\rangle$$

and neglect terms of the order of or higher than $1/I$.

A similar procedure can be used to derive $M1$ transitions from one-phonon wobbling band into the yrast band. Ignoring the terms of the order of I^{-1} in Eq. (A.11) in the high-spin limit ($I \approx K \gg 1$), we have the following approximative values for the Clebsch–Gordan coefficients in terms of the matrix elements of the operators B and $B^\dagger$ (or $\hat{Q}_{wobb}$ and $\hat{Q}^\dagger_{wobb}$):

$$(I\,K\,1\,0\,|\,I\,K) \to 1,$$
$$(I\,K\,1\,0\,|\,I \pm 1\,K) \to$$
$$\to \pm\frac{1}{\sqrt{I}}\left\langle n \pm 1 \left| \begin{array}{c} B^\dagger \\ B \end{array} \right| n \right\rangle,$$
$$(I\,K\,1 \pm 1\,|\,I\,K \pm 1) \to$$
$$\to \mp\frac{1}{\sqrt{I}}\left\langle n \mp 1 \left| \begin{array}{c} B \\ B^\dagger \end{array} \right| n \right\rangle,$$
$$(I\,K\,1 \pm 1\,|\,I \pm 1\,K \pm 1) \to 1.$$
$$\quad (A.16)$$

Because $\langle\hat{\mathcal{M}}(M1\,\nu_1 = \pm 1)\rangle = 0$, we obtain

$$\langle I'K'n'_w||\hat{\mathcal{M}}(M1\,\nu_1 = 0)||IKn_w\rangle =$$
$$= \sqrt{2I+1}\langle n'_w|\left[\delta_{I',I}\langle\hat{\mathcal{M}}(M1, \nu_1 = 0)\rangle +\right.$$
$$+ \delta_{I',I+1}\frac{1}{\sqrt{I}}\langle\hat{\mathcal{M}}(M1, \nu_1 = 0)\rangle(x\hat{Q}^\dagger_{wobb} + y\hat{Q}_{wobb}) -$$
$$\left.- \delta_{I',I-1}\frac{1}{\sqrt{I}}\langle\hat{\mathcal{M}}(M1, \nu_1 = 0)\rangle(x\hat{Q}_{wobb} + y\hat{Q}^\dagger_{wobb})\right] \times$$
$$\times |n_w\rangle, \quad (A.17)$$

where

$$\hat{\mathcal{M}}(M1; \nu_1) = \mu_N \sqrt{3} \times$$
$$\times \sum_{i=1}^A \left(\frac{1}{2}g_s^{(i,eff)}[\sigma \otimes Y_{l=0}]_{1\nu_1} + g_l^{(i,eff)}[l \otimes Y_{l=0}]_{1\nu_1}\right)$$

is the magnetic dipole operator. With the aid of Eqs. (A.7), (A.8), and (A.12) and the definition of operators given in Ref. [21], we obtain the expression

$$B(M1; I n_w \to I \pm 1 \text{ yr}) = \left|\langle\hat{M}^{(M)}_{1\nu_3=1}[r = +1]\rangle\right|^2 \times$$
$$\times \frac{1}{4I}\frac{\left(\sqrt{W_3} \mp \sqrt{W_2}\right)^2}{\sqrt{W_2 W_3}} \quad (A.18)$$

for $M1$ transitions from the one-phonon wobbling band ($n_w = 1$) into the yrast band ($n_w = 0$). The magnetic moment $\langle\hat{M}^{(M)}_{1\nu_3=1}[+]\rangle$ can be calculated in any microscopic model.

REFERENCES

1. A. Bohr and B. R. Mottelson, *Nuclear Structure*, Vol. II, Benjamin, New York (1975).

2. S. G. Nilsson and I. Ragnarsson, *Shapes and Shells in Nuclear Structure*, Cambridge Univ. Press, Cambridge (1995).

3. P. G. Reinhard, V. O. Nesterenko, E. Suraud et al., Phys. Rev. A **66**, 013206 (2002).

4. I. Bialynicki-Birula and T. Sowinski, Phys. Rev. A **71**, 043610 (2005).

5. I. N. Mikhailov and D. Janssen, Phys. Lett. B **72**, 303 (1978).

6. D. Janssen, I. N. Mikhailov, R. G. Nazmitdinov et al., Phys. Lett. B **79**, 347 (1978).

7. Y. R. Shimizu and M. Matsuzaki, Nucl. Phys. A **588**, 559 (1995).

8. D. Janssen and I. N. Mikhailov, Nucl. Phys. A **318**, 390 (1979).

9. E. R. Marshalek, Nucl. Phys. A **331**, 429 (1979).

10. S. W. Ødegård et al., Phys. Rev. Lett. **86**, 5866 (2001); D. R. Jensen et al., Phys. Rev. Lett. **89**, 142503 (2002), Nucl. Phys. A **703**, 3 (2002); H. Amro et al., Phys. Lett. **553B**, 197 (2003); G. Schönwasser et al., Phys. Lett. B **552**, 9 (2003); A. Görgen et al., Phys. Rev. C **69**, 031301(R) (2004); D. R. Jensen et al., Eur. Phys. J. A **19**, 173 (2004).

11. I. Hamamoto, Phys. Rev. C **65**, 044305 (2002); I. Hamamoto and G. B. Hagemann, Phys. Rev. C **67**, 014319 (2003).

12. M. Matsuzaki, Y. R. Shimizu, and K. Matsuyanagi, Phys. Rev. C **65**, 041303(R) (2002).

13. M. Matsuzaki, Y. R. Shimizu, and K. Matsuyanagi, Phys. Rev. C **69**, 034325 (2004).

14. http://www.nndc.bnl.gov/nudat2/.

15. F. G. Kondev et al., Phys. Lett. **437B**, 35 (1998).

16. J. Kvasil and R. G. Nazmitdinov, Pis'ma v ZhETF **83**, 227 (2006) [JETP Lett. **83**, 187 (2006)]; Phys. Rev. C **73**, 014312 (2006).

17. J. Kvasil, N. Lo Iudice, R. G. Nazmitdinov et al., Phys. Rev. C **69**, 064308 (2004).

18. R. F. Casten, E. A. McCutchan, N. V. Zamfir et al., Phys. Rev. C **67**, 064306 (2003).

19. T. Nakatsukasa, K. Matsuyanagi, S. Mizutori, and Y. R. Shimizu, Phys. Rev. C **53**, 2213 (1996).

20. J. Kvasil and R. G. Nazmitdinov, Fiz. Elem. Chastits At. Yadra **17**, 613 (1986) [Sov. J. Part. Nucl. **17**, 265 (1986)].

21. J. Kvasil, N. Lo Iudice, V. O. Nesterenko, and M. Kopál, Phys. Rev. C **58**, 209 (1998).

22. R. Wyss, W. Satula, W. Nazarewicz, and A. Johnson, Nucl. Phys. A **511**, 324 (1990).

23. H. Sakamoto and T. Kishimoto, Nucl. Phys. A **501**, 205 (1989).

24. W. D. Heiss and R. G. Nazmitdinov, Pis'ma v ZhETF **72**, 157 (2000) [JETP Lett. **72**, 106 (2000)]; Phys. Rev. C **65**, 054304 (2002).

25. R. G. Nazmitdinov, D. Almehed, and F. Dönau, Phys. Rev. C **65**, 041307(R) (2002).

26. P. Ring and P. Schuck, *The Nuclear Many-Body Problem*, Springer-Verlag, New York (1980).

27. E. R. Marshalek, Nucl. Phys. A **275**, 416 (1977).

28. D. A. Varshalovich, A. N. Moskalev, and V. K. Khersonskii, *Quantum Theory of Angular Momentum*, World Sci., Singapore (1986).

29. D. Almehed, F. Dönau, and R. G. Nazmitdinov, J. Phys. G **29**, 2193 (2003).

30. S. Frauendorf, Rev. Mod. Phys. **73**, 463 (2001).

31. R. G. Nazmitdinov, Yad. Fiz. **46**, 732 (1987) [Sov. J. Nucl. Phys. **46**, 412 (1987)].

32. E. R. Marshalek, Nucl. Phys. A **266**, 317 (1976).

33. I. Hamamoto, Nucl. Phys. A **271**, 15 (1976).

34. A. Bohr and B. R. Mottelson, *Nuclear Structure*, Vol. I, Benjamin, New York (1969).